

# A Central Catecholaminergic Circuit Controls Blood Glucose Levels during Stress

## Highlights

- VLM CA neurons are essential for stress-induced hyperglycemia
- Activation of VLM CA neurons induces hyperglycemia via projections to the spinal cord
- VLM CA neurons receive direct inputs from multiple stress-related brain areas
- The PVN provides excitatory inputs to VLM CA neurons and regulates hyperglycemia

## Authors

Zhe Zhao, Liang Wang,  
Wenling Gao, ..., Sen Song,  
Minmin Luo, Cheng Zhan

## Correspondence

zhancheng@nibs.ac.cn

## In Brief

Zhao et al. identified a neural circuit that controls blood glucose levels during stress. They demonstrate that VLM CA neurons integrate stress signals from multiple stress-related areas (e.g., the PVN) and cause hyperglycemia via descending projections to the spinal cord.

# A Central Catecholaminergic Circuit Controls Blood Glucose Levels during Stress

Zhe Zhao,<sup>1,8</sup> Liang Wang,<sup>1,8</sup> Wenling Gao,<sup>1,8</sup> Fei Hu,<sup>1</sup> Juen Zhang,<sup>1</sup> Yuqi Ren,<sup>1,5</sup> Rui Lin,<sup>1,5</sup> Qiru Feng,<sup>1,6</sup> Mingxiu Cheng,<sup>7</sup> Dapeng Ju,<sup>1,4</sup> Qingsheng Chi,<sup>3</sup> Dehua Wang,<sup>3,9</sup> Sen Song,<sup>7,9</sup> Minmin Luo,<sup>1,2,9</sup> and Cheng Zhan<sup>1,9,10,\*</sup>

<sup>1</sup>National Institute of Biological Sciences, Beijing, 102206, China

<sup>2</sup>School of Life Sciences, Tsinghua University, Beijing 100084, China

<sup>3</sup>State Key Laboratory of Integrated Management for Pest Insects and Rodents, Institute of Zoology, Chinese Academy of Sciences, Beijing 100101, China

<sup>4</sup>College of Biological Science, China Agricultural University, Beijing, 100193, China

<sup>5</sup>PTN Graduate Program, School of Life Sciences, Peking University, Beijing 100081, China

<sup>6</sup>PTN Graduate Program, School of Life Sciences

<sup>7</sup>Department of Biomedical Engineering, Center for Brain-inspired Computing Research, McGovern Institute for Brain Research Tsinghua University, Beijing 100084, China

<sup>8</sup>These authors contributed equally

<sup>9</sup>Senior author

<sup>10</sup>Lead Contact

\*Correspondence: zhancheng@nibs.ac.cn

<http://dx.doi.org/10.1016/j.neuron.2017.05.031>

## SUMMARY

Stress-induced hyperglycemia is a fundamental adaptive response that mobilizes energy stores in response to threats. Here, our examination of the contributions of the central catecholaminergic (CA) neuronal system to this adaptive response revealed that CA neurons in the ventrolateral medulla (VLM) control stress-induced hyperglycemia. Ablation of VLM CA neurons abolished the hyperglycemic response to both physical and psychological stress, whereas chemogenetic activation of these neurons was sufficient to induce hyperglycemia. We further found that CA neurons in the rostral VLM, but not those in the caudal VLM, cause hyperglycemia via descending projections to the spinal cord. Monosynaptic tracing experiments showed that VLM CA neurons receive direct inputs from multiple stress-responsive brain areas. Optogenetic studies identified an excitatory PVN-VLM circuit that induces hyperglycemia. This study establishes the central role of VLM CA neurons in stress-induced hyperglycemia and substantially expands our understanding of the central mechanism that controls glucose metabolism.

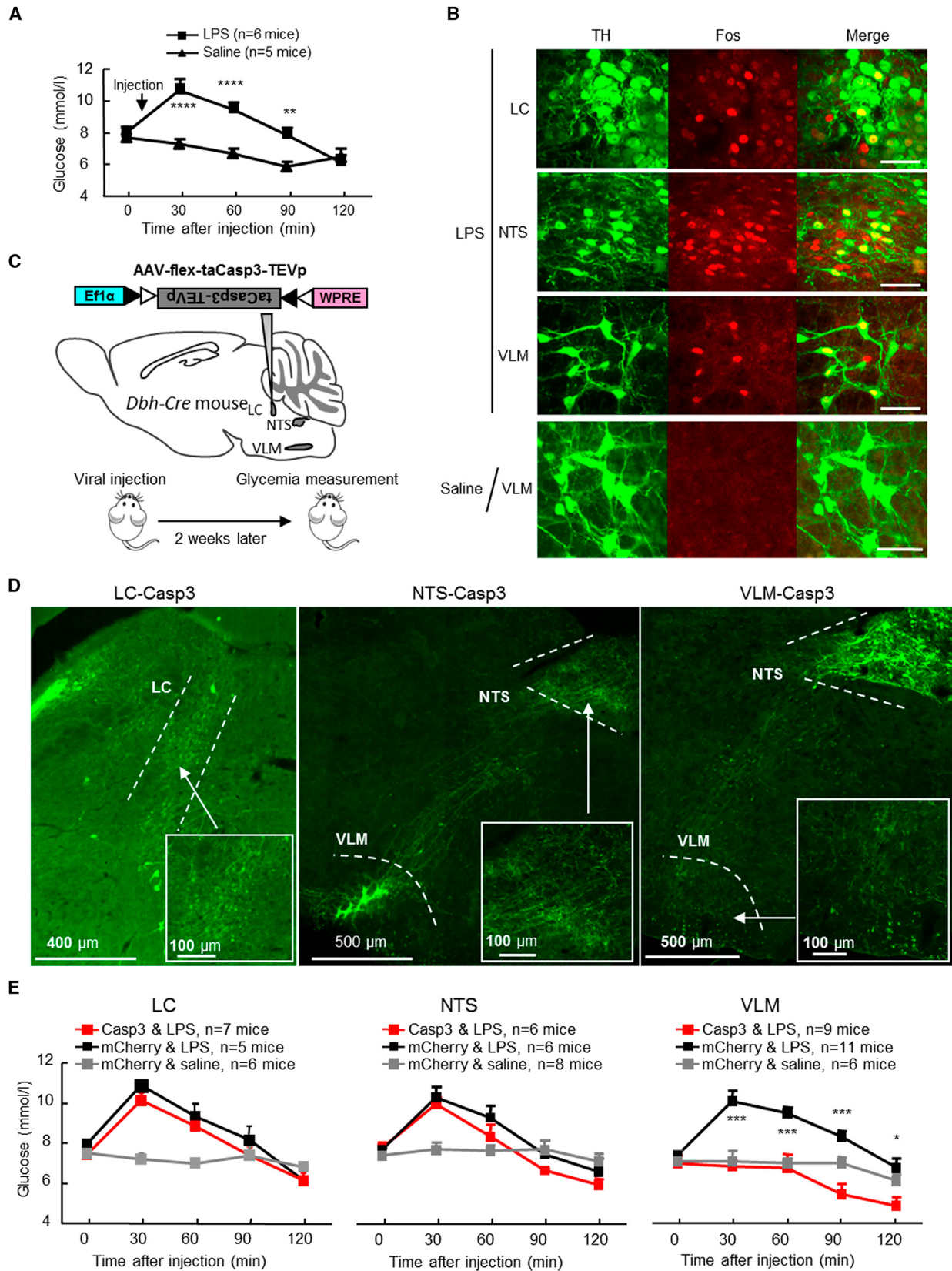
## INTRODUCTION

Glucose is the main energy source for mammals. When facing significant threats (stressors), the body's glucose stores are mobilized, resulting in a rapid elevation of blood glucose levels. This stress-induced hyperglycemia provides a quickly accessible energy supply for animals in danger with which to under-

take the proverbial fight-or-flight response, thereby promoting an individual's survival (Marik and Bellomo, 2013). Many brain areas, including hypothalamic regions and the hindbrain, have previously been shown to regulate both blood glucose levels and stress responses (Ulrich-Lai and Ryan, 2014). However, the key brain site responsible for stress-induced hyperglycemia has not been established.

Hindbrain catecholaminergic (CA) neurons (here referring specifically to norepinephrine and epinephrine neurons) are known to be highly responsive to various stressors, including immobilization and immune challenges (Ericsson et al., 1994; Kvetnansky et al., 2009; Morilak et al., 2005; Stanford, 1995). The locus coeruleus (LC) is the major pool of central CA neurons. Electrophysiological recordings in freely moving cats showed that most LC CA neurons are activated by hypoglycemia and are inhibited following glucose administration (Morilak et al., 1987), suggesting a role for LC CA neurons in glucoregulatory responses. Indeed, the LC-CA system has actually been proposed to drive the sympathetic nervous system and thereby cause stress-induced hyperglycemia (Marik and Bellomo, 2013).

Outside the LC, CA neurons are also located in the nucleus tractus solitaires (NTS) and in the ventrolateral medulla (VLM) (Kfelt et al., 1974; Moore and Bloom, 1979). Glucose-sensing neurons have been identified in the NTS (Adachi et al., 1995; Ballfour et al., 2006), and activation of NTS neurons expressing glucose transporter 2 increased glucagon secretion (Lamy et al., 2014). VLM CA neurons have been previously shown to regulate hyperglycemia. Immunotoxic ablation of CA neurons in the rostral part of the VLM abrogates hyperglycemia, adrenaline secretion, and adrenal medullary Fos expression in response to the glucoprivive agent 2-deoxy-D-glucose (Madden et al., 2006; Ritter et al., 2001). Local microinjection of the GABA<sub>A</sub> receptor antagonist bicuculline into the VLM induces hyperglycemia, an effect dependent on intact adrenal glands (Verberne and Sartor, 2010). Although separate populations of CA neurons have been shown to be important in glucose homeostasis, the



(legend on next page)

question of whether or not the central CA system is involved in stress-induced hyperglycemia remains open.

In the present study, we used a cell-type-specific ablation approach to survey the roles of three different populations (LC, NTS, and VLM) of central CA neurons in stress-induced hyperglycemia. Strikingly, we found that only the VLM CA population is indispensable in controlling stress-induced hyperglycemia. Moreover, the selective activation of VLM CA neurons induced hyperglycemia via descending projections to the spinal cord. We then mapped the whole-brain monosynaptic inputs of VLM CA neurons and found that these neurons receive direct inputs from many stress-related nuclei. Specifically, we found that the hypothalamic paraventricular nucleus (PVN) sends excitatory projections to the VLM and causes hyperglycemia.

## RESULTS

### VLM CA Neurons Are Essential in Mediating Both Physical and Psychological Stress-Induced Hyperglycemia

Stressors commonly used in animal studies are classified into at least two categories: physical stress (also referred to as homeostatic or systemic, e.g., infection) and psychological stress (also referred to as emotional or neurogenic, e.g., footshock or restraint) (Dayas et al., 2001; Pacák and Palkovits, 2001). While some brain areas are known to be activated by both types of stress, neural circuits involved in processing stress responses are category specific (Dayas et al., 2001; Sawchenko et al., 2000). To examine whether the CA neural system is important in mediating stress-induced hyperglycemia, we initially challenged animals with a physical stressor, bacterial lipopolysaccharide (LPS), to induce acute hyperglycemia; LPS has a long history of use as an immune stress treatment (Lang et al., 1985). Injection of LPS significantly increased blood glucose levels in C57BL/6J mice (Figure 1A), confirming the suitability of LPS for inducing acute hyperglycemia. To check whether the CA neural system is activated by LPS challenge, Fos expression was examined as an indicator of neuronal activation. Immunoreactivity to tyrosine hydroxylase (TH) was used as a marker of hindbrain CA neuron identity. Following LPS challenge, Fos expression was observed within subsets of TH-immunoreactive neurons, including those in the LC, NTS, and VLM (Figure 1B), suggesting that these groups of CA neurons are responsive to LPS stress signals.

We next checked whether the neuronal activity of these CA neurons is required for the manifestation of LPS-induced hyperglycemia by performing a loss-of-function study that used a genetic approach to ablate particular CA neuronal populations in adult mice. Briefly, a Cre-dependent AAV vector encoding a genetically engineered Casp3 gene (AAV-flex-taCasp3-TEVp) was bilaterally injected into the LC, NTS, or VLM of *Dbh-Cre* transgenic mice (referred to as *Dbh-LC<sup>Casp3</sup>*, *Dbh-NTS<sup>Casp3</sup>*, and *Dbh-VLM<sup>Casp3</sup>* mice, respectively) (Figure 1C). Casp3 activation has been shown to induce cell apoptosis (Yang et al., 2013; Zhang et al., 2016). *Dbh-Cre* mice express the Cre recombinase under the control of the promoter the dopamine-β-hydroxylase (*Dbh*) gene. *Dbh* is a rate-limiting enzyme for the synthesis of the catecholamines NE and E and is expressed only in CA cells (Gerfen et al., 2013). Here, Casp3 was selectively expressed in CA neurons, and this resulted in cell-type-specific ablation. As a negative control, an AAV-DIO-mCherry vector was injected into the LC, the NTS, or the VLM of *Dbh-Cre* mice (referred to as *Dbh-LC<sup>mCherry</sup>*, *Dbh-NTS<sup>mCherry</sup>*, and *Dbh-VLM<sup>mCherry</sup>* mice, respectively) (Figure S1A). Two weeks after the viral injections, TH immunostaining was performed to confirm the ablation. A majority (~90%) of the CA neurons in the targeted LC, NTS, or VLM areas were selectively ablated (number of remaining CA neurons:  $24 \pm 5$  neurons in *Dbh-LC<sup>Casp3</sup>* mice [ $n = 7$ ] versus  $1,892 \pm 143$  neurons in *Dbh-LC<sup>mCherry</sup>* mice [ $n = 6$ ];  $220 \pm 27$  in *Dbh-NTS<sup>Casp3</sup>* mice [ $n = 6$ ] versus  $1,301 \pm 43$  in *Dbh-NTS<sup>mCherry</sup>* mice [ $n = 8$ ];  $110 \pm 35$  in *Dbh-VLM<sup>Casp3</sup>* mice [ $n = 9$ ] versus  $987 \pm 32$  in *Dbh-VLM<sup>mCherry</sup>* mice [ $n = 11$ ]; mean  $\pm$  SEM). Importantly, only the deliberately targeted areas of *Dbh-Cre* mice were selectively ablated; the CA cell populations of the other brain areas remained intact (Figure 1D), demonstrating the anatomical precision of the ablation.

We then examined whether the ablation of CA neurons affected stress-induced hyperglycemia. Although the LC is known to be the major CA neuronal pool and has for a long time been implicated in stress responses (Aston-Jones and Bloom, 1981), the bilateral ablation of LC CA neurons had no significant effect on LPS-induced hyperglycemia (Figure 1E, left). Similarly, the ablation of NTS CA neurons did not alter LPS-induced hyperglycemia (Figure 1E, middle). In contrast, the selective ablation of VLM CA neurons eliminated the expected LPS-induced hyperglycemia (Figure 1E, right). Interestingly, mice lacking VLM CA neurons exhibit hypoglycemia after LPS treatments, suggesting that energy stores may not be quickly mobilized to restore the glucose that is consumed by the

### Figure 1. The VLM Catecholaminergic Neuronal Population Plays a Central Role in Controlling LPS-Induced Hyperglycemia

(A) Immune stress (LPS, 10 µg/kg bodyweight, IP injection, black arrowhead) induced an acute hyperglycemic response. Control mice (saline, IP injection) did not exhibit hyperglycemia. \*\* $p < 0.01$ , \*\*\* $p < 0.0001$ ; two-way ANOVA analyses followed by Bonferroni's post hoc test. Data represent means  $\pm$  SEM in this and following figures.

(B) Injection of LPS, but not saline, elicited Fos expression (red) in tyrosine hydroxylase (TH)-expressing neurons (green) within the LC, NTS, and VLM. Expression of TH is a marker for hindbrain catecholaminergic (CA) neurons. Fos and TH double-labeled cell number:  $74 \pm 5$  (LPS) versus  $1 \pm 0.5$  (saline) in the LC;  $194 \pm 8$  (LPS) versus  $3.5 \pm 1$  (saline) in the NTS;  $289 \pm 5$  (LPS) versus  $11 \pm 3$  (saline) in the VLM;  $n = 3$  mice for each group. Scale bar: 50 µm.

(C) Cartoon illustrating the loss-of-function strategy used in this study.

(D) CA neurons restricted within the LC (left), NTS (middle), or VLM (right) were selectively ablated following injection of AAV-flex-Casp3-TEVp. TH immunostaining (green) was performed to confirm the ablation. White rectangular areas in each image show zoomed-in views of the areas indicated by arrows.

(E) Ablating CA neurons in the VLM (right), but not the LC (left) or the NTS (middle), eliminated LPS-induced hyperglycemia. \* $p < 0.05$ , \*\*\* $p < 0.001$ ; two-way ANOVA analyses followed by Bonferroni's post hoc test between *Dbh-VLM<sup>Casp3</sup>* and *Dbh-VLM<sup>mCherry</sup>* mice following LPS treatment.

See also Figure S1.

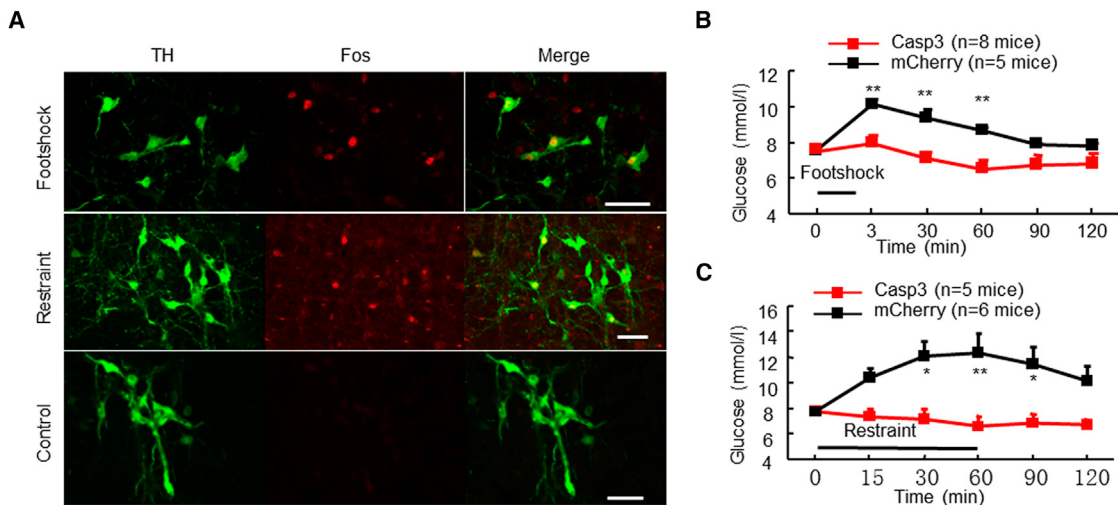


**Figure 2. VLM CA Neurons Are Required for Both Footshock- and Restraint-Induced Hyperglycemia**

(A) Both footshock (0.5 mA, 2 s duration with 6 s interval, for 3 min) and restraint (1 hr) stress elicited Fos expression (red) in TH-expressing neurons (green) within the VLM. Scale bar: 50  $\mu$ m.

(B and C) Selectively ablating VLM CA neurons eliminated both footshock- (B) and restraint- (C) induced hyperglycemia. The duration of stress is indicated with a horizontal bar. \*\* $p$  < 0.01; two-way ANOVA analyses followed by Bonferroni's post hoc test.

immune system. Note that VLM-ablation had no significant effect on basal blood glucose levels ( $7.03 \pm 0.29$  mmol/L of *Dbh-VLM*<sup>Casp3</sup> mice [ $n = 9$ ] versus  $7.48 \pm 0.17$  mmol/L of *Dbh-VLM*<sup>mCherry</sup> mice [ $n = 11$ ], mean  $\pm$  SEM). These results indicate that CA neurons in the VLM, but not those in the LC or the NTS, are essential for LPS-induced hyperglycemia.

To examine whether VLM CA neurons are required for mediating hyperglycemic responses caused by psychological stressors, we challenged mice both with electric footshock and with restraint stress. Both brief footshock (0.5 mA, 2 s duration with a 6 s interval, for 3 min) and restraint (1 hr) activated VLM CA neurons (Figure 2A). These results suggest that VLM CA neurons also process psychological stress-induced responses. Importantly, ablation of VLM CA neurons abolished both footshock- and restraint-induced hyperglycemia (Figures 2B and 2C). The ablation of CA neurons in the LC or the NTS had no effect on footshock-induced hyperglycemia (Figures S1B and S1C). Our LPS, footshock, and restraint results all support the conclusion that VLM CA neurons are essential for stress-induced hyperglycemia.

We next asked whether silencing VLM CA neurons without ablating them can block stress-induced hyperglycemia. A Cre-dependent AAV vector encoding the *Guillardia theta* anion channelrhodopsin1 (GtACR1) (Govorunova et al., 2015), a recently developed optogenetic inhibition tool, was bilaterally injected into the VLM of *Dbh-Cre* mice (Figure 3A). Blue light (473 nm) illumination could robustly silence GtACR1/GFP-positive neurons, and these neurons could recover to their basal firing rate within 3 s after photostimulation (Figures 3B and 3C). Moreover, photostimulation of GtACR1-expressing neurons did not significantly alter the resting membrane potential ( $-71.7 \pm 4.5$  mV pre laser illumination versus  $-73.1 \pm 4.1$  mV post laser illumination,  $n = 4$  neurons, mean  $\pm$  SEM) (Figure 3D). Consistent with our ablation results, light inhibition of VLM CA

neurons largely blocked hyperglycemic responses under all three of the stress treatments (Figures 3E and 3F), further confirming that VLM CA neurons are necessary for stress-induced hyperglycemia.

#### Activation of VLM CA Neurons Is Sufficient to Increase Blood Glucose Levels

To examine whether direct activation of VLM CA neurons alone can increase blood glucose levels, we used the DREADD method (designer receptors exclusively activated by designer drugs) to selectively activate these neurons (Alexander et al., 2009). A Cre-dependent AAV vector encoding both the hM3Dq receptor (a high-affinity receptor for the pharmacologically inert ligand clozapine-N-oxide [CNO]) and the red fluorescent protein mCherry (AAV-DIO-hM3Dq-mCherry) was injected into the VLM of *Dbh-Cre* mice (*Dbh-VLM*<sup>hM3Dq</sup> mice) (Figure 4A). The hM3Dq/mCherry signals were colocalized with TH immunoreactivity in the majority (>95%, 3,670 neurons from 5 *Dbh-VLM*<sup>hM3Dq</sup> mice) of VLM neurons (Figure 4B). Following CNO administration, Fos expression and Ca<sup>2+</sup> transients in hM3Dq/mCherry-expressing neurons confirmed the suitability of the DREADD method for the experimental activation of VLM CA neurons, both *in vivo* and *in vitro* (Figures 4C and S2, see also STAR Methods).

We examined whether the activation of VLM CA neurons affects blood glucose levels. IP injection of CNO into *Dbh-VLM*<sup>hM3Dq</sup> mice significantly increased blood glucose levels within 30 min. Owing to the relatively long duration of the pharmacological action of CNO (Alexander et al., 2009), glucose levels continued to rise, reaching a plateau within 2 hr (Figure 4D), before returning to baseline within 6 hr (data not shown). In contrast, the injection of saline did not alter blood glucose levels in *Dbh-VLM*<sup>hM3Dq</sup> mice. As an additional control, the injection of CNO into *Dbh-VLM*<sup>mCherry</sup> mice did not alter blood glucose levels

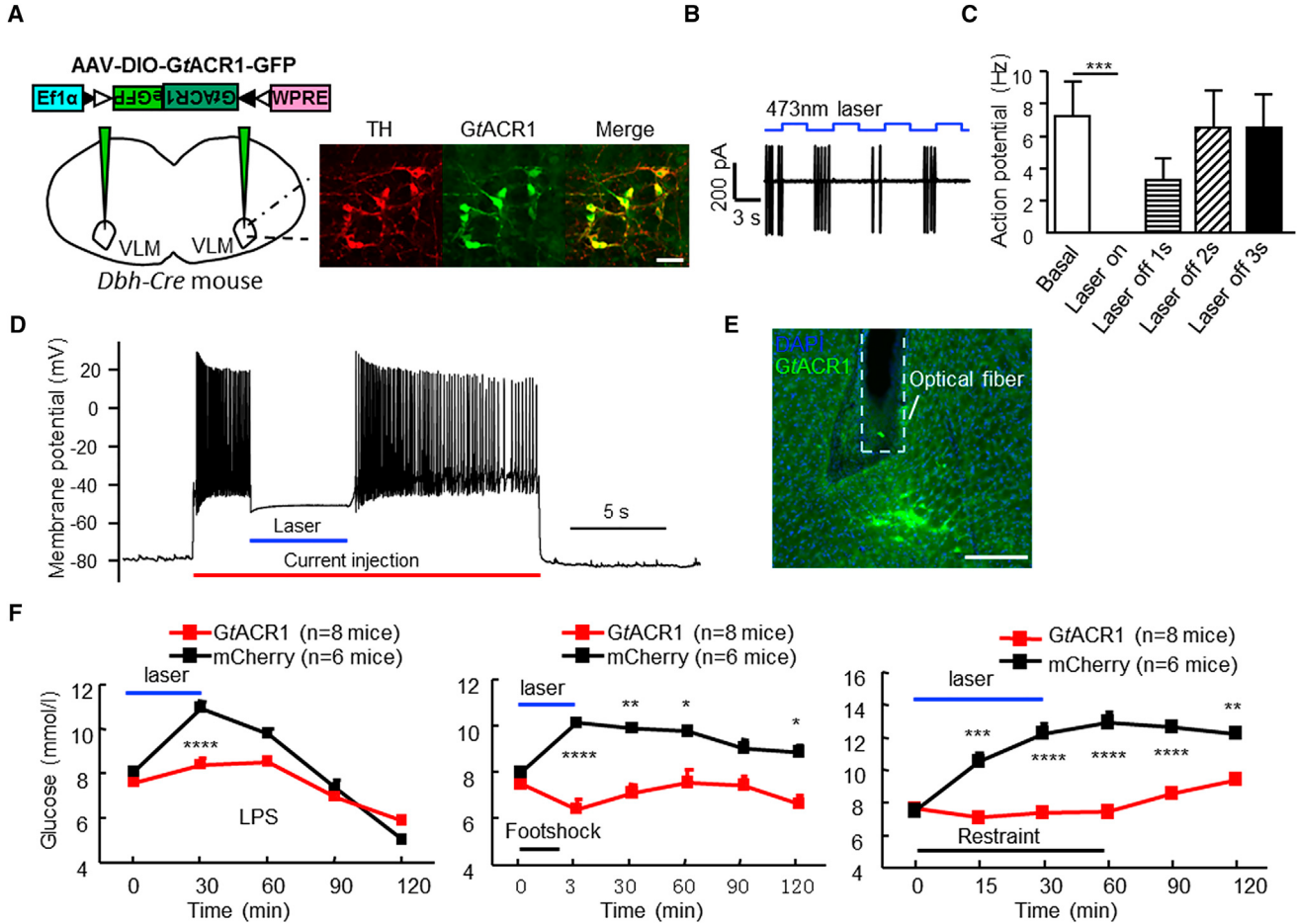


**Figure 3. Optogenetic Inhibition of VLM CA Neurons Largely Blocked Stress-Induced Hyperglycemia**

(A) For acute silencing VLM CA neurons, AAV-DIO-GtACR1-GFP was bilaterally injected into the VLM of *Dbh-Cre* mice (left). Two weeks after the injection, GtACR1 (green) was selectively expressed in VLM TH-immunoreactive (red) neurons (right). Scale bar: 50  $\mu$ m.

(B and C) Cell-attached slice recording shows that blue light (473 nm laser, 3 s on, 3 s off) completely silenced GtACR1-expressing neurons. (C) Group data ( $n = 4$  neurons) shows that neurons recover to their basal firing rate within 3 s after light inhibition. \*\*\* $p < 0.001$ ; paired Student's t test.

(D) Raw trace from a representative GtACR1-expressing neuron showing that blue laser illumination (473 nm, blue bar) inhibited action potentials evoked by the injection of depolarizing current (40 pA, red bar), without altering the resting membrane potential.

(E) A representative image showing the optical fiber placement (white solid line) in the VLM of a *Dbh-VLM<sup>GtACR1</sup>* mouse. Scale bar: 200  $\mu$ m.

(F) Light inhibition of VLM CA neurons largely blocked LPS- (left), footshock- (middle), and restraint- (right) induced hyperglycemia. \* $p < 0.05$ , \*\* $p < 0.01$ , \*\*\* $p < 0.001$ , \*\*\*\* $p < 0.0001$ ; two-way ANOVA analyses followed by Bonferroni's post hoc test.

either (Figure 4D). The selective activation of CA neurons in the LC or NTS did not increase blood glucose levels (Figure S3). These results strongly support the notion that VLM CA neurons are sufficient to induce hyperglycemia.

#### The Adrenal Glands Serve as Peripheral Mediators of VLM CA Neurons in Controlling Stress-Induced Hyperglycemia

It is well known that stress increases blood glucose levels by stimulating the release of stress hormones from the adrenal glands. We examined whether VLM CA neurons control glucose levels by regulating the activity of the adrenal glands. Chemogenetic activation of VLM CA neurons significantly increased serum epinephrine and corticosterone levels (Figures 4E). Following the

bilateral removal of the adrenal glands from *Dbh-VLM<sup>hM3Dq</sup>* mice, the basal epinephrine and corticosterone levels in adrenalectomized mice were extremely low, and injection of CNO did not increase the levels of either stress hormone (Figure 4F). Importantly, bilateral adrenalectomy completely blocked the hyperglycemia elicited by activating VLM CA neurons (Figure 4G). There was no significant difference in the blood glucose levels between CNO- and saline-treated adrenalectomized *Dbh-VLM<sup>hM3Dq</sup>* mice (two-way ANOVA: Time  $F(4,48) = 0.1846$ ,  $p = 0.9453$ ; injections  $F(1,12) = 1.741$ ,  $p = 0.2116$ ; interaction between time and injections  $F(4,48) = 1.242$ ,  $p = 0.3059$ ). Consistent with these chemogenetic activation results, the ablation of VLM CA neurons nearly abolished the stress-induced increases of these two hormones (Figure 4H). These results show that

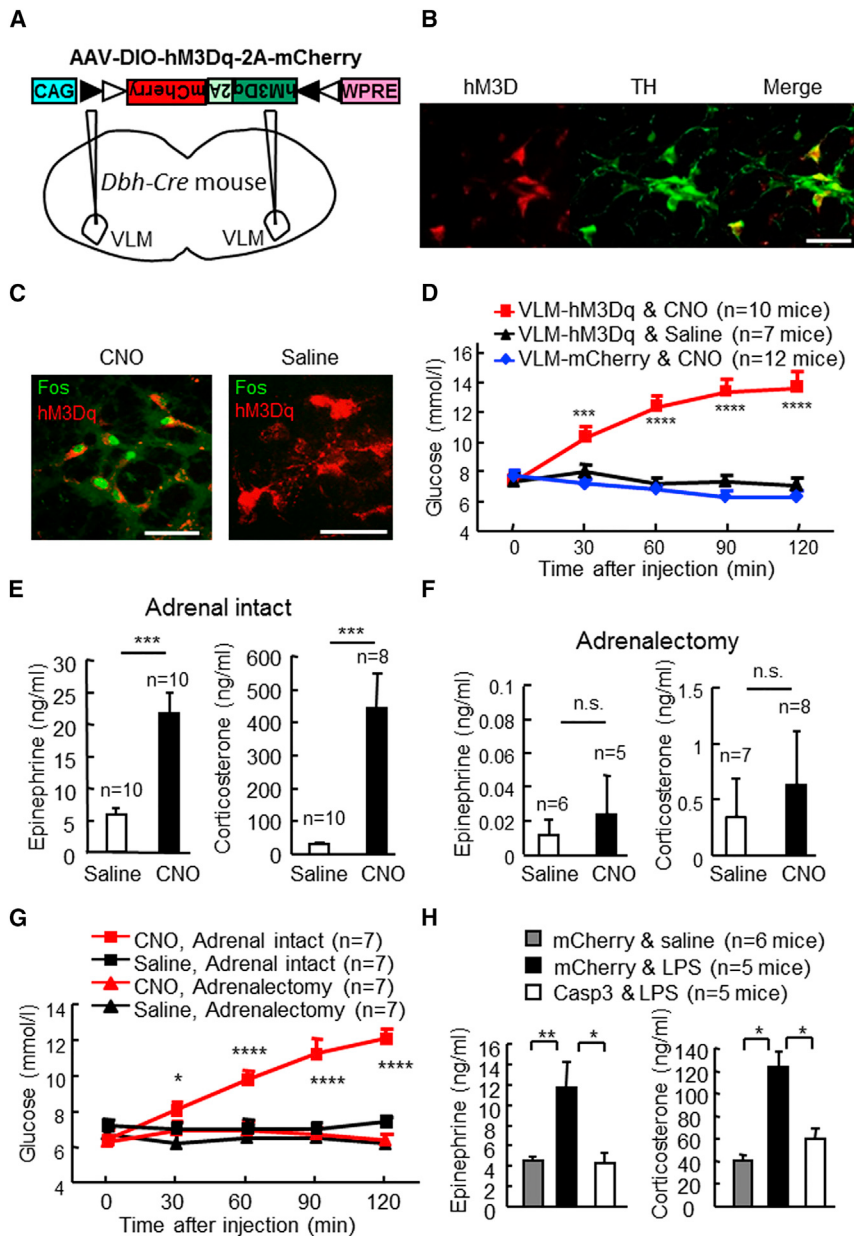


**Figure 4. Activation of VLM CA Neurons Rapidly Increases Blood Glucose Levels**

(A) For acute activation of VLM CA neurons, AAV-DIO-hM3Dq-mCherry was bilaterally injected into the VLM of *Dbh-Cre* mice.

(B) Two weeks after the viral injection, hM3Dq/mCherry (red) was selectively expressed in VLM TH-immunoreactive (green) neurons. Scale bar: 50 μm.

(C) Following the expression of hM3Dq/mCherry in VLM CA neurons, the injection of CNO (1 mg/kg bodyweight, IP, left), but not the injection of saline (right), elicited Fos expression (green) in hM3Dq+ neurons (red). Cell number of Fos-positive neurons: 406 ± 148 in 791 ± 307 hM3Dq/mCherry neurons (n = 5 mice, CNO 1 mg/kg bodyweight, IP injection); 1 ± 0.5 Fos-positive neurons in 522 ± 147 hM3Dq/mCherry neurons (n = 4 mice, saline, IP injection). Scale bar: 50 μm.

(D) Blood glucose levels of *Dbh-VLM<sup>hM3Dq</sup>* and *Dbh-VLM<sup>mCherry</sup>* mice following injection of CNO (1 mg/kg bodyweight, IP) or saline. \*\*\*p < 0.001, \*\*\*\*p < 0.0001; two-way ANOVA analyses followed by Bonferroni's post hoc test between CNO and saline treatments in *Dbh-VLM<sup>hM3Dq</sup>* mice.

(E and F) Injection of CNO increased serum epinephrine and corticosterone levels in adrenal-intact (E), but not in adrenalectomized (F), *Dbh-VLM<sup>hM3Dq</sup>* mice. \*\*\*p < 0.001, n.s., not significant; unpaired Student's t test.

(G) Bilateral adrenalectomy abolished the blood glucose increase induced by activation of VLM CA neurons. \*p < 0.05, \*\*\*p < 0.0001; two-way ANOVA analyses followed by Bonferroni's post hoc test between CNO and saline treatments in *Dbh-VLM<sup>hM3Dq</sup>* mice.

(H) Serum epinephrine (left) and corticosterone (right) levels in *Dbh-VLM<sup>mCherry</sup>* and *Dbh-VLM<sup>Casp3</sup>* mice following injection of LPS or saline. \*p < 0.05, \*\*p < 0.01, unpaired Student's t test.

See also Figures S2 and S3.

the adrenal glands can be viewed as peripheral, downstream effectors of VLM CA neurons in mediating stress-induced hyperglycemia.

### VLM CA Neurons Increase Blood Glucose Levels via Descending Projections to the Spinal Cord

To identify neural circuits recruited by VLM CA neurons to increase blood glucose levels, we used a Cre-dependent, cell-type-specific anterograde AAV viral tracer (AAV-DIO-mGFP) to examine the projection patterns of these neurons (Figures 5A and 5B). VLM CA neurons send outputs to 28 brain areas, including intense projections in the spinal intermediolateral nucleus (IML), the NTS, the LC, the dorsomedial hypothalamic nucleus, the paraventricular thalamic nucleus, the PVN, and the

ventromedial preoptic nucleus (Figure 5C and Table S1, n = 5 mice). It is known that the preganglionic neurons of the sympathetic nervous system are located in the spinal IML and the PVN is the head of the hypothalamic-pituitary-adrenal (HPA) axis (Sawchenko and Swanson, 1982; Ulrich-Lai and Herman, 2009). Given the importance of both the sympathetic nervous system and the HPA axis in stress responses, we examined the precise distribution patterns of spinally and PVN-projecting neurons by injecting Texas red-conjugated dextran amine (MW = 3KD, TR3K), a retrograde tracer, into the PVN or the IML (T8-T11) (Figure 5D). We found that the majority of PVN-projecting CA neurons were located in the caudal ventrolateral medulla (CVLM) (Figures 5E, S4C, and S4E). In contrast, nearly all spinally projecting VLM CA neurons were located in the rostral ventrolateral medulla (RVLM, Bregma -6.8 mm~-6.2 mm) (Figures 5E, S4D, and S4F). There were few overlapping distributions between spinally projecting neurons and PVN-projecting neurons, suggesting that individual

VLM CA neurons appear not to collaterally project to both the PVN and IML.

To further confirm this seeming lack of collateralization, we employed classical dual-color retrograde labeling methods to determine whether individual CA neurons in the VLM are able to project to both the PVN and the IML. A given mouse was injected with two retrograde tracers: Cholera toxin b-subunit conjuncted with Alexa 488 (CTb-488) was injected into the PVN; TR3K was injected into the IML (Figures 5F, S4A, and S4B). We did not detect any TH-immunoreactive neurons ( $n = 5$  mice) in the VLM that had been double-labeled by both CTb-488 and TR3K (Figures 5G and 5H). It can therefore be concluded that the distinct projections to the spinal cord and to the PVN arise from two separate populations of VLM CA neurons.

To assess the discreet contributions of the RVLM and the CVLM CA neuron populations to the regulation of hyperglycemia, hM3Dq/mCherry+ was selectively expressed in RVLM CA neurons by delivering a small volume (100 nL) of AAV-DIO-hM3Dq-mCherry into the RVLM of *Dbh-Cre* mice (referred to as *Dbh-RVLM<sup>hM3Dq</sup>* mice). The majority of hM3Dq/mCherry+ neurons were located in the RVLM (Figure S5A, labeled  $236 \pm 44$  neurons in the RVLM and  $41 \pm 16$  hM3Dq/mCherry+ neurons in the CVLM,  $n = 6$  mice, mean  $\pm$  SEM). Injecting CNO into the *Dbh-RVLM<sup>hM3Dq</sup>* mice significantly increased blood glucose levels (Figure 5I). Moreover, transection of the thoracic spinal cords of these mice prevented communication between the VLM to the IML, thus blocking the hyperglycemic response (Figure 5I). In contrast, after selectively expressing hM3Dq/mCherry+ in CVLM CA neurons (Figure S5B, 0 hM3Dq/mCherry+ neurons in the RVLM and  $338 \pm 23$  hM3Dq/mCherry+ neurons in the CVLM,  $n = 7$  mice, mean  $\pm$  SEM), the injection of CNO did not induce hyperglycemia (Figure 5J). These results suggest that CA neurons in the RVLM, but not those in the CVLM, are sufficient to induce hyperglycemia.

We performed a Pearson correlation analysis between the number of surviving CA neurons (from the ablation experiments, Figures 1 and 2) and the blood glucose level increase values resulting from LPS challenge. Consistent with results of chemogenetic experiments, this analysis indicated that the increase of blood glucose levels was positively correlated with the number of surviving CA neurons in the RVLM ( $r = 0.75$ ,  $p = 0.0005$ ), but not with the number of surviving CA neurons in the CVLM ( $r = 0.39$ ,  $p = 0.11$ ) (Figures S5C and S5D), suggesting that the CA neurons in the RVLM, but not those in the CVLM, are required for induction of hyperglycemia.

We next asked whether RVLM CA neurons induced hyperglycemia via projections to the spinal cord. A recently developed AAV variant, that enables retrograde access to projection neurons (Tervo et al., 2016) was used to selectively express a light-sensitive cation channel ChannelRhodopsin 2 (ChR2) in spinally projecting RVLM CA neurons following the injection of rAAV2-retro-Cre-GFP into the spinal cord and the injection of AAV-DIO-ChR2-mCherry into the RVLM (Figures 5K and 5L). We found that light stimulation of the spinally projecting RVLM CA neurons rapidly induced hyperglycemia (Figure 5M). In contrast, no changes in blood glucose levels were observed when we selectively expressed ChR2 in the VLM CA neurons

of *Dbh-Cre* mice and stimulated the ChR2-expressing CA terminals in the PVN with light (Figures S5E–S5I). These results show that RVLM CA neurons increase blood glucose levels via descending projections to the spinal cord rather than via ascending projections to the PVN.

### VLM CA Neurons Receive Inputs from Stress-Responsive Neurons

To examine how VLM CA neurons are activated, and to gain a global perspective on the sources of their excitatory inputs, we examined the monosynaptic inputs of these neurons using a Cre-dependent, modified rabies virus-based whole-brain tracing strategy (see STAR Methods) (Wang et al., 2015; Wickersham et al., 2007). In total,  $263 \pm 50$  (mean  $\pm$  SEM,  $n = 4$  mice) VLM CA neurons received direct input from  $8,915 \pm 3,562$  (mean  $\pm$  SEM,  $n = 4$  mice) neurons distributed in 38 brain areas (Figure 6A). The strongest labeling was observed in the medulla, including the NTS, the intermediate reticular nucleus, the gigantocellular reticular nucleus, and the medullary reticular nucleus (Figure 6A). Outside of the medulla, major inputs arose from the lateral parabrachial nucleus (LPB) and the Kölliker-Fuse nucleus in the pons, from the periaqueductal gray (PAG) and the dorsal raphe nucleus (DRN) in the midbrain, from the PVN and the dorsomedial hypothalamic nucleus (DMH) in the hypothalamus, and from two other areas: the bed nucleus of the stria terminalis (BNST) and the central amygdaloid nucleus (CeA) (Figures 6A and 6B).

We next examined whether these brain areas provide excitatory inputs to the VLM by injecting CTb-488 into the VLM and AAV-DIO-mCherry into those upstream nuclei of *Slc17a6-ires-Cre* mice (Figure 6C). *Slc17a6* (also known as *Vglut2*) encodes a glutamate synaptic vesicle transporter VGLUT2 that is expressed in the PVN (Vong et al., 2011). Hence mCherry was selectively expressed in excitatory neurons. We found many neurons located in the DMH, LPB, DRN, and lateral hypothalamus (LH) were double labeled by CTb488 and mCherry (i.e., glutamatergic) (Figure 6D), suggesting that these brain areas provide excitatory inputs to the VLM. In contrast, none of CTb-488 back-labeled neurons in the CeA and BNST were positive for mCherry (Figures S6D and S6E). Remarkably, many upstream brain areas of the VLM are well-known stress-related nuclei such as the PVN, LPB, LH, and DMH (Ericsson et al., 1994; Stotz-Potter et al., 1996; Ulrich-Lai and Herman, 2009).

We verified that these input areas convey stress signals to the VLM. One week following injecting CTb-488 into the VLM, the mice were subsequently subjected to LPS or footshock stress treatments, and Fos expression was examined in CTb-488-labeled neurons. Both LPS and footshock induced the expression of Fos in CTb-488 back-labeled neurons in the PVN and in other stress-related nuclei (Figures 6E and 6F), indicating that many VLM-projecting neurons are indeed activated by stress. Collectively, these results strongly suggest that VLM CA neurons integrate stress signals from multiple upstream stress-responsive neurons.

### An Excitatory PVN to VLM CA Neuron Circuit that Increases Blood Glucose Levels

Given the vast number of studies implying a central role for the PVN in stress responses, we used ChR2-assisted circuit

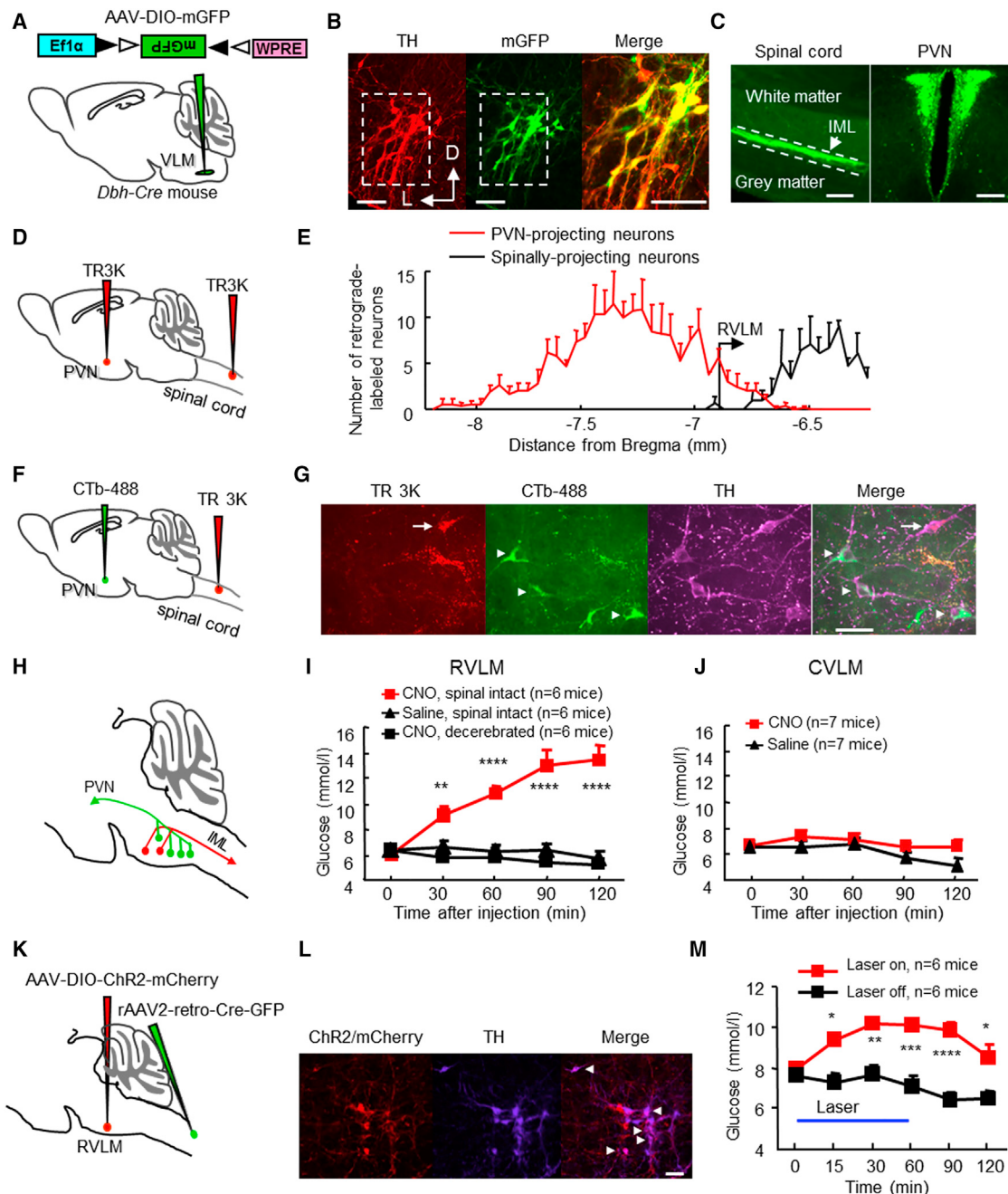


**Figure 5. VLM CA Neurons Increase Blood Glucose Levels via Descending Projections to the Spinal Cord**

(A) For whole-brain anterograde tracing, a Cre-dependent AAV vector encoding membrane GFP (mGFP) was unilaterally delivered into the VLM of *Dbh-Cre* mice.

(B) Selective expression of mGFP (green) in TH-expressing (red) neurons within the VLM following the injection of AAV-DIO-mGFP. Right panel shows the overlay of mGFP signals and TH immunoreactivity within the dashed rectangle area in the two left panels. D, dorsal; L, lateral. Scale bar: 100 μm.

(C) VLM-derived intense CA axon projections to the spinal IML (left, indicated by a triangle) and the PVN (right). Scale bar: 200 μm.

(D) For retrograde tracing, TR3K was injected into the PVN or IML.

(E) The distribution profiles of retrogradely labeled PVN-projecting VLM CA neurons (red line, total 951 neurons from 4 mice) and spinally projecting VLM CA neurons (black line, total 185 neurons from 3 mice).

(F) Dual-color retrograde tracing with CTb-488 and TR3K. CTb-488 was injected into the PVN, and TR3K was injected into the IML.

(G) Representative image showing that none of the TH-immunoreactive (purple, Alexa 647) neurons (n = 5 mice) were double labeled by both CTb-488 (green) and TR3K (red) in the VLM. The arrow indicates a TR3K and TH-immunoreactive double-labeled neuron. The triangles indicate CTb-488 and TH-immunoreactive double-labeled neurons. Scale bar: 40 μm.

(legend continued on next page)

mapping to study the functional effect(s) of the monosynaptic projections from the PVN to VLM CA neurons (Figure 7A). PVN-derived ChR2/mCherry-expressing axons were found in the VLM, and axonal swellings were observed to be closely associated with CA neuronal somas (Figures 7B and 7D). Following injection of AAV-DIO-ChR2-mCherry into the PVN of *Slc17a6-ires-Cre* mice (referred to as *Slc17a6-PVN<sup>ChR2</sup>* mice) and CTb-488 into the VLM, about half of CTb-488 back-labeled neurons (1,221 neurons from 2 mice) in the PVN expressed ChR2/mCherry (Figure 7C), suggesting that the PVN sends excitatory projections to the VLM. To examine whether PVN glutamatergic neurons provide monosynaptic inputs to VLM CA neurons, we generated *Slc17a6-Cre::Th-GFP* mice by crossing *Slc17a6-Cre* and *Th-GFP* mouse lines. Following injection of AAV-DIO-ChR2-mCherry into the PVN of *Slc17a6-Cre::Th-GFP* mice, electrophysiological recordings in brain slices showed that RVLM CA neurons receive monosynaptic excitatory inputs from the PVN (Figures 7E–7G). Taken together, these results demonstrate that PVN glutamatergic neurons project to VLM CA neurons.

Bilateral light stimulation of the glutamatergic nerve endings in the RVLM of *Slc17a6-PVN<sup>ChR2</sup>* mice rapidly increased blood glucose levels (<15 min) (Figure 7H). Notably, this increase was accompanied by an anorexic effect (Figure S7H). In contrast, light stimulation did not induce hyperglycemia in control *Slc17a6-PVN<sup>mCherry</sup>* mice (Figure 7H). These results suggest that activation of PVN-derived glutamatergic inputs in the VLM is sufficient to induce hyperglycemia. We subsequently examined the necessity of the PVN-VLM circuit in mediating stress-induced hyperglycemia. AAV-DIO-GtACR1-GFP was injected into the PVN of *Slc17a6-ires-Cre* mice (referred to as *Slc17a6-PVN<sup>GtACR1</sup>* mice) (Figure 7I). Optogenetic inhibition of PVN-derived glutamatergic nerve endings in the VLM did not impair the stress-induced hyperglycemic response (Figures 7J–7L), suggesting that the PVN-VLM circuit may not be essential for stress-induced hyperglycemia.

The PVN contains separate populations of neurosecretory neurons that secret different peptide hormones such as oxytocin (Oxt), arginine vasopressin (Avp), thyrotropin-releasing hormone (Trh), and corticotropin-releasing hormone (Crh). To examine whether PVN Crh neurons project to the VLM, CTb-488 was injected into the VLM, and AAV-DIO-mCherry was injected into the PVN of *Crh-ires-Cre* mice. *Crh-ires-Cre* mice have Cre recombinase expression in Crh neurons, hence mCherry was

selectively expressed in Crh neurons (Taniguchi et al., 2011). About 10% (168 mCherry neurons in 1,678 CTb-488-labeled neurons, n = 2 mice) CTb-488 back-labeled neurons were mCherry positive (i.e., Crh neurons), suggesting that PVN Crh neurons project to the VLM (Figure S7A). Following injection of CTb-488 into the VLM, we examined immunoreactivity of CTb-488 back-labeled neurons to these peptide hormones in the PVN. We found that about 10% of the CTb-488 back-labeled neurons were Oxt-immunoreactive in the PVN (163 Oxt-positive neurons among 1,897 CTb-488 labeled neurons, n = 2 mice) (Figure S7B). None of the back-labeled VLM-projecting neurons were positive for Avp (0 Avp-positive neurons among 1,680 CTb-488-labeled neurons, n = 2 mice) (Figure S7C). To determine whether PVN Trh neurons project to the VLM, we examined Trh mRNA expression in the PVN following injection of rAAV2-hSyn-retro-eGFP into the VLM and found that exceedingly few GFP-positive neurons in the PVN expressed Trh mRNA (2 Trh mRNA-expressing neurons among 1,204 GFP positive neurons, n = 3 mice) (Figure S7D). These results appear to exclude the involvement of Avp and Trh neurons in the PVN from PVN-VLM hyperglycemic pathway.

We then injected AAV-DIO-mGFP into the PVN of *Crh-ires-Cre* or *Oxt-ires-Cre* (Cre recombinase is expressed in Oxt neurons) (Wu et al., 2012), which further confirmed that both Crh and Oxt neurons send projections to the VLM (Figure S7E). Next, we examined the effects of these projections on blood glucose levels. AAV-DIO-ChR2-mCherry was injected into the PVN of *Oxt-ires-Cre* or *Crh-ires-Cre* mice (Figure S7F). However, optogenetic activation of axonal projections in the VLM showed that neither Crh nor Oxt projections could induce hyperglycemia (Figure S7G), suggesting that these projections maybe affect other functions rather than blood glucose levels.

## DISCUSSION

We demonstrate here that VLM CA neurons play a central role in stress-induced hyperglycemia. First, ablation of VLM CA neurons eliminated stress-induced hyperglycemia, whereas activation of these neurons rapidly increased blood glucose levels. Second, RVLM CA neurons induced hyperglycemia via descending projections to the spinal cord in a sympathetic-adrenal-pathway manner. Third, monosynaptic tracing and functional neuroanatomical experiments showed that many stress-responsive nuclei convey stress signals to the VLM. Optogenetic

(H) Cartoon summarizing the retrograde tracing results. Two separate populations of VLM CA neurons project, respectively, to the PVN (green) and spinal IML (red).

(I) Selective activation of rostral VLM CA neurons increased blood glucose levels; this effect was blocked following spinal transection. \*\*p < 0.01, \*\*\*p < 0.0001; two-way ANOVA analyses followed by Bonferroni's post hoc test between CNO and saline treatments in *Dhb-RVLM<sup>M3Dq</sup>* mice. ANOVA analysis of saline injections in spinal-intact animals and CNO injections in decerebrate animals: Time F(4,40) = 2.335, p = 0.072; Injections F(1,10) = 3.084, p = 0.109; interaction between time and type of injection F(4,40) = 0.986, p = 0.425.

(J) Selective activation of caudal VLM CA neurons did not increase blood glucose levels. There was no significant difference between the CNO and saline treatments. Two-way ANOVA: injection type F(1,11) = 3.002, p = 0.11.

(K) For selectively stimulating spinally projecting RVLM CA neurons, AAV-retro-Cre-GFP was injected into the spinal cord, and AAV-DIO-ChR2-mCherry was injected into the RVLM.

(L) ChR2/mCherry (red) and TH-immunoreactive (purple, Alexa 647) double-labeled neurons (indicated by triangles) in the RVLM. Scale bar: 50 μm.

(M) Optogenetic activation of spinally projecting RVLM CA neurons increased blood glucose levels. \*p < 0.05, \*\*p < 0.01, \*\*\*p < 0.001, \*\*\*\*p < 0.0001; two-way ANOVA analyses followed by Bonferroni's post hoc test.

See also Figures S4 and S5.

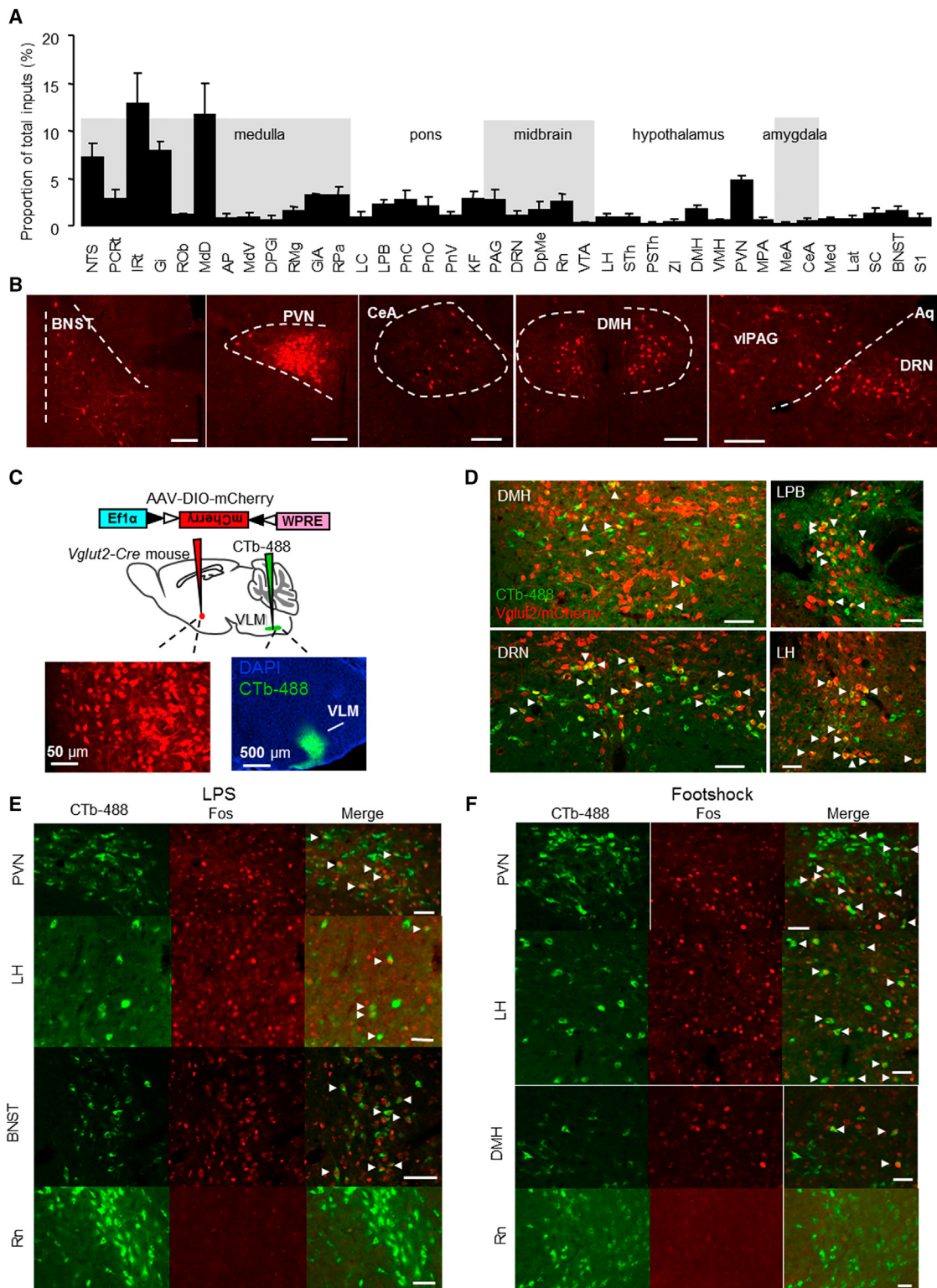


**Figure 6. VLM CA Neurons Receive Direct Inputs from Stress-Responsive Neurons**

(A) Percentage of whole-brain monosynaptic inputs to VLM CA neurons. The values are the normalized ratios of the cell number in each area against the total number of input neurons. n = 4 mice.

(legend continued on next page)

activation of the excitatory projections from the PVN to the VLM resulted in hyperglycemia. Our study demonstrates that VLM-mediated circuits control stress-induced hyperglycemia (Figure 7M) and provides insights into how the brain maintains adequate energy during periods of stress.

### VLM CA Neurons Are Required for Both Physical and Psychological Stress-Induced Hyperglycemia

Different types of stress activate distinctive patterns of neuronal activation in the brain (Dayas et al., 2001; Herman and Cullinan, 1997; Li et al., 1996). For example, a comparison of neuronal activation patterns observed in response to acute immune and footshock challenges reveals them to generally be quite distinct (Sawchenko et al., 2000). However, there might be common nuclei or circuits accounting for a given stress response, regardless of the types of stressors. In agreement with this idea, we found that selective ablation or inhibition of VLM CA neurons blocked the hyperglycemic response to LPS, footshock, and restraint stress.

Prior studies have shown the importance of VLM CA neurons in responses to acute cerebral glucose deficit. Selective killing of particular subsets of CA neurons in the hindbrain (e.g., those of the VLM and the LC) can attenuate the hyperglycemic response to the glucoprivic agent 2-DG (Madden et al., 2006; Ritter et al., 2001). However, given that VLM CA neurons are widely conserved in mammals, and considering their powerful role in regulating hyperglycemia, it seems unlikely that these neurons only deal with acute, profound glucose deficits that occur very rarely (Ritter et al., 2011). Although previous studies elegantly highlighted the importance of VLM CA neurons in controlling glucoregulatory responses, the fact that their methods simultaneously ablated a substantial proportion of CA neurons from multiple brain areas made it exceedingly difficult to directly attribute the attenuation of a particular glucoregulatory response to single populations of CA cells. By taking advantage of the improved anatomical precision of recently developed genetic ablation and inhibition techniques, we were here able to identify the essential role of the VLM CA neuronal population in stress-induced hyperglycemia.

Neuronal populations in the hypothalamus have been identified as being crucial for maintaining basal energy metabolism and glucose homeostasis (Morton et al., 2006). Ablations of hypothalamic neurons dramatically disrupt basal energy metabolism and lead to glycemic disorders (Gropp et al., 2005; Luquet et al., 2005; Zhan et al., 2013). In contrast with ablation of hypothalamic neurons, ablation of VLM CA neurons did not alter basal blood glucose levels. Our findings support the idea that the

hypothalamus and brainstem function differentially in the regulation of energy metabolism.

### The LC-CA System Is Dispensable in Mediating Stress-Induced Hyperglycemia

Although the LC-CA system is typically viewed as a major component of the centrally mediated fight-or-flight response, our results demonstrate that the LC-CA system is neither essential nor sufficient for initiating stress-induced hyperglycemia. In contrast to VLM CA neurons, which send heavy projections to the HPA axis and the sympathetic nervous system (Kvetnansky et al., 2009; Moore and Bloom, 1979; Rinaman, 2010), the LC sends intense projections to high cognitive centers such as the hippocampus and the cortex but sends few inputs to the PVN or the spinal cord (Moore and Bloom, 1979; Sawchenko and Swanson, 1982). Therefore, although the LC-CA system has been implicated in many stress-induced neuropsychiatric disorders such as anxiety, depression, and post-traumatic stress (McCall et al., 2015; Sara, 2009; Southwick et al., 1997; Sun et al., 2015), the role of the LC-CA system in controlling stress-induced hyperglycemia appears to be indirect or dispensable.

### VLM CA Neurons Mobilize Energy Stores via the Sympathetic-Adrenal System

Local microinjection of bicuculline into the VLM induces hyperglycemia (Verberne and Sartor, 2010). However, the general complexity and the diversity of cell types of the VLM have made it extremely difficult to assign conventional causal pharmacological roles to a specific type of neuron in the VLM. Here, we provided direct evidence that VLM CA neurons are sufficient to induce hyperglycemia.

Two foundational studies showed that VLM CA neurons have axonal projections into the spinal cord and other forebrain regions (Hökfelt et al., 1973; Kfet et al., 1974). However, no studies have provided direct evidence to characterize the (possibly varied) functional roles of projections toward particular regions. Using optogenetic tools in combination with a retrograde AAV variant, we here conclusively establish that the RVLM-spinal circuit is sufficient to induce hyperglycemia.

Increases in the hepatic output of glucose have been proposed as the primary mechanism underlying stress-induced hyperglycemia (Dungan et al., 2009). Consistently, we show here that activation of VLM CA neurons resulted in significantly higher hepatic expression of glucose-6-phosphatase (G6pc) and phosphoenolpyruvate carboxykinase 1 (Pepck), two key genes that regulate glycogenolysis and gluconeogenesis (Figure S2B).

(B) Examples of stress-related brain areas that provide direct input to VLM CA neurons. Montage images were acquired and stitched on an Olympus VS120 microscope. Scale bar: 200  $\mu$ m.

(C and D) For labeling excitatory inputs of the VLM, CTb-488 was injected into the VLM (green, bottom right), and AAV-DIO-ChR2-mCherry was injected into its upstream brain areas (red, bottom left) of *Slc17a6-Cre* mice (C). Representative images showing many doubled-labeled neurons (indicated by triangles) in the DMH, LPB, DRN, and LH (D). Scale bar: 50  $\mu$ m.

(E) Representative images showing Fos immunoreactivity in CTb-488 back-labeled neurons from the VLM, as elicited by LPS treatment. Fos and CTb-488 double-labeled neurons (indicated by triangles) were observed in the PVN, LH, and BNST, but not the red nucleus (Rn). Scale bar: 50  $\mu$ m.

(F) Representative images showing Fos immunoreactivity in CTb-488 back-labeled neurons from the VLM, as elicited by footshock. Fos and CTb-488 double-labeled neurons (indicated by triangles) were observed in the PVN, LH, and DMH, but not the red nucleus (Rn). Scale bar: 50  $\mu$ m.

See also Figure S6 and Table S1.

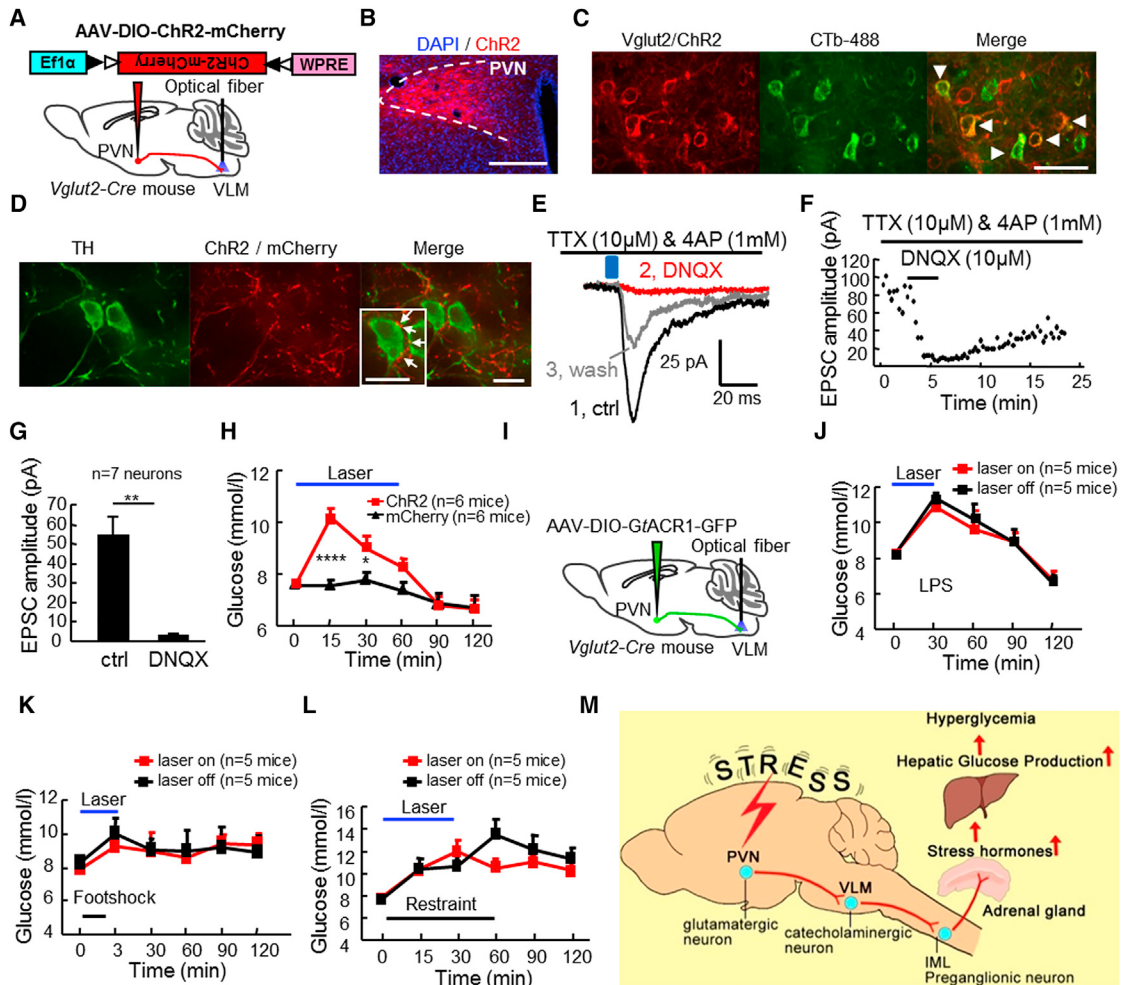


**Figure 7. PVN-Derived Glutamatergic Projection in the VLM Is Sufficient, but Not Required, to Induce Hyperglycemia**

(A) In vivo optogenetic experiment to selectively activate the PVN-derived glutamatergic projections in the VLM.

(B) Representative image showing ChR2/mCherry-expressing neurons (red) following injection of a Cre-dependent vector AAV-DIO-ChR2-mCherry into the PVN of *Slc17a6*-Cre mice. Scale bar: 200 μm.

(C) Representative image showing CTb-488 and ChR2/mCherry double-labeled neurons (indicated by triangles) in the PVN following injection of CTb-488 into the VLM and injection of AAV-DIO-ChR2-mCherry into the PVN of *Slc17a6*-Cre mice. Scale bar: 50 μm.

(D) PVN-derived ChR2/mCherry-expressing glutamatergic axonal swellings (arrowheads) apposed to TH-immunoreactive cell bodies (green) in the VLM. Scale bar: 20 μm.

(E–G) PVN glutamatergic neurons provide monosynaptic inputs to VLM CA neurons. Raw traces of whole-cell recordings (E) show that the excitatory postsynaptic currents (EPSCs) evoked by light stimulation (blue bar, 5 ms) (1) were abolished by application of the AMPA-type glutamate receptor blocker DNQX (10 μM) (2), and the currents can be partially impaired by washing with ACSF (3), demonstrating that the observed evoked-currents are glutamatergic in nature. (F) shows a time-series plot of the EPSC amplitude draw data from one representative cell, and (G) shows group data (n = 7 cells). All recordings were performed during the application of TTX (10 μM) and 4-AP (1 mM), demonstrating that VLM CA neurons received monosynaptic input from PVN. \*\*p < 0.01, paired Student's t test. (H) Light stimulation (5-ms duration, 20 Hz, 1 s on, 1 s off for 1 hr, horizontal bar) of PVN-derived glutamatergic nerve endings in the VLM rapidly increased blood glucose levels. \*p < 0.05, \*\*\*p < 0.0001. Two-way ANOVA analyses followed by Bonferroni's post hoc test between *Slc17a6*-PVN<sup>ChR2</sup> and *Slc17a6*-PVN<sup>mCherry</sup> mice: animal groups F(1,10) = 10.78, p = 0.0437; time F(5,50) = 22.99, p < 0.001; interaction between time and animal groups F(5,50) = 8.504, p < 0.001.

(I) In vivo optogenetic experiment to selectively inhibit the PVN-derived glutamatergic projections in the VLM.

(J–L) Optogenetic inhibition of PVN-derived glutamatergic projections in the VLM did not decrease LPS- or footshock-induced hyperglycemia, although it had a minor but not significant effect on restraint-induced hyperglycemia. Two-way ANOVA analyses followed by Bonferroni's post hoc test.

(M) Schematic VLM-mediated circuits for stress-induced hyperglycemia. Stress signals activate multiple brain areas, including the PVN. PVN glutamatergic neurons provide a direct excitatory input to VLM CA neurons and thereby stimulate the release of stress hormones, which in turn increase hepatic glucose production and eventually lead to hyperglycemia.

See also Figure S7.

Therefore, VLM-mediated hyperglycemia may be predominantly resulted from the breakdown of hepatic glycogen (Figure 7M).

RVLM CA neurons are known to regulate a range of unique autonomic functions (Guyenet et al., 2013; Ritter et al., 2006). Abbott et al. demonstrated that optogenetic activation of RVLM CA neurons in conscious mice increased breathing rates and affected cardiorespiratory functions (Abbott et al., 2013); other studies have shown the influences of RVLM CA neurons on glucoprivic responses and arterial pressure (Madden et al., 2006; Ritter et al., 2001). Electrophysiological recording in the RVLM has identified at least two types of RVLM CA neurons with different axonal conduction velocities (Schreihofner and Guyenet, 1997). Verberne et al. found that RVLM neurons that respond to 2-DG administration are not barosensitive, whereas RVLM barosensitive neurons were either unaffected or slightly inhibited by 2-DG administration (Verberne and Sartor, 2010). Additionally, our retrograde tracing results establish that there are at least two separate populations of RVLM CA neurons: PVN-projecting neurons and spinally projecting neurons. Although it is unclear whether the neurons and circuits characterized in the present study may have the capacity to control other functions, a preponderance of evidence suggests subpopulations of RVLM CA neurons probably function differentially in controlling autonomic responses.

### The Upstream Inputs into VLM CA Neurons

The VLM CA neuronal population, in particular the rostral part (i.e., RVLM), has been proposed to function as an emergency center in the brain (Guyenet et al., 2013). A recent work showed that RVLM CA neurons were necessary and sufficient for stress-induced ischemia-reperfusion protection, which elegantly highlights the importance of these neurons in dealing with emergency (Abe et al., 2017). In support of the “emergency center” hypothesis for VLM CA neurons, our monosynaptic retrograde tracing study showed that these neurons receive direct inputs from multiple stress-related nuclei, suggesting that VLM CA neurons do indeed occupy a key position for the integration of stress signals.

We found that the PVN is a nucleus of stress signaling that functions upstream of the VLM to inhibit food intake and cause hyperglycemia. The role of the PVN in controlling appetite is now well established. For example, subsets of PVN glutamatergic neurons provide excitatory inputs to agouti-related protein neurons in the arcuate nucleus and thereby drive hunger (Krashes et al., 2014). Whereas selective suppression of PVN axon projections to the vIPAG/DRN elicited feeding (Stachniak et al., 2014), food intake was suppressed following the activation of the PVN-LPB (Garfield et al., 2015). Beyond appetite and feeding, Kalsbeek et al. demonstrated that pharmacological activation of PVN neurons can cause hyperglycemia (Kalsbeek et al., 2004), although the precise circuitry through which the PVN induces hyperglycemia has remained obscure. The present study helps to clarify this, as we show that the PVN-VLM circuit is necessary for the induction of hyperglycemia.

Following endotoxin treatments, the peripheral immune system can activate the NTS via the afferent vagus (Ek et al., 1998), which then activates downstream areas to trigger behavioral and physiological responses (Ericsson et al., 1994). The NTS sends heavy projections to the PVN (Rinaman, 2010), which

may ultimately relay stress signals to the VLM. Alternatively, the NTS is also known to send direct inputs to the VLM (Sawchenko and Swanson, 1982). Therefore, consistent with the assumption that stress signals may activate VLM CA neurons via multiple circuits, the PVN-VLM circuit is sufficient, but not necessary, to induce hyperglycemia.

Stress-related glycemic disorders increase many health risk factors for both diabetics and non-diabetic people (Bradley, 1988; McCowen et al., 2001). For example, stress-induced hyperglycemia is frequently observed in critically ill patients and likely contributes to poor clinical outcomes (Capes et al., 2000; Dungan et al., 2009). Intensive insulin therapy is often used for strict control of blood glucose levels in intensive care units, but this carries the risk of inducing hypoglycemic episodes (Marik and Bellomo, 2013; Xiu et al., 2014). Our study establishes that blood glucose levels during stress are tightly controlled by VLM CA neurons and identifies the particular neural circuits that function in this regulatory process.

### STAR★METHODS

Detailed methods are provided in the online version of this paper and include the following:

- KEY RESOURCES TABLE
- CONTACT FOR REAGENT AND RESOURCE SHARING
- EXPERIMENTAL MODEL AND SUBJECT DETAILS
- METHOD DETAILS
  - Production of viral vectors
  - Stereotaxic virus and tracer injections
  - Glucose, corticosterone, and epinephrine measurement
  - Real-time PCR
  - Optogenetic experiments
  - Adrenalectomy and spinal transection
  - Electrophysiological Recordings and Calcium Imaging
  - Histology and immunoassaying
  - RNA in situ hybridization
- QUANTIFICATION AND STATISTICAL ANALYSIS

### SUPPLEMENTAL INFORMATION

Supplemental Information includes seven figures and one table and can be found with this article online at <http://dx.doi.org/10.1016/j.neuron.2017.05.031>.

### AUTHOR CONTRIBUTIONS

Z.Z., L.W., and W.G. performed imaging experiments and behavioral assays. F.H., J.Z., and Y.R. performed physiological recordings. Q.F. and R.L. prepared AAV vectors. M.C. performed *in situ* hybridization experiments. D.J. performed the real-time PCR experiments. Z.Z. and C.Z. analyzed the data. D.W., S.S., and Q.C. contributed reagents and laboratory equipment. C.Z. designed the experiments. C.Z. and M.L. wrote the manuscript.

### ACKNOWLEDGMENTS

We thank Dr. Karl Deisseroth (Stanford University) for the AAV-DIO-ChR2-mCherry construct, Dr. Dongsheng Duan (University of Missouri) for technical advice on the packing of the AAV virus, Ping Wu (NCPSB) for imaging assistance, and Drs. Tao Wang and Erquan Zhang (NIBS) for advice concerning

manuscript preparation. M.L. is supported by grants from the MOST (2012CB837701 and 2012YQ03026005) and the NSFC (91432114) of China, and by funding from the Beijing Municipal Government. C.Z. is supported by grants from the MOST (2012CB837703) and the NSFC (31500860) of China, and by funding from the Beijing Municipal Government.

Received: October 11, 2016

Revised: March 24, 2017

Accepted: May 22, 2017

Published: June 15, 2017

## REFERENCES

- Abbott, S.B., DePuy, S.D., Nguyen, T., Coates, M.B., Stornetta, R.L., and Guyenet, P.G. (2013). Selective optogenetic activation of rostral ventrolateral medullary catecholaminergic neurons produces cardiorespiratory stimulation in conscious mice. *J. Neurosci.* 33, 3164–3177.
- Abe, C., Inoue, T., Inglis, M.A., Viar, K.E., Huang, L., Ye, H., Rosin, D.L., Stornetta, R.L., Okusa, M.D., and Guyenet, P.G. (2017). C1 neurons mediate a stress-induced anti-inflammatory reflex in mice. *Nat. Neurosci.* 20, 700–707.
- Adachi, A., Kobashi, M., and Funahashi, M. (1995). Glucose-responsive neurons in the brainstem. *Obes. Res.* 3 (Suppl 5), 73S–740S.
- Alexander, G.M., Rogan, S.C., Abbas, A.I., Armbruster, B.N., Pei, Y., Allen, J.A., Nonneman, R.J., Hartmann, J., Moy, S.S., Nicolelis, M.A., et al. (2009). Remote control of neuronal activity in transgenic mice expressing evolved G protein-coupled receptors. *Neuron* 63, 27–39.
- Aston-Jones, G., and Bloom, F.E. (1981). Norepinephrine-containing locus coeruleus neurons in behaving rats exhibit pronounced responses to non-noxious environmental stimuli. *J. Neurosci.* 1, 887–900.
- Balfour, R.H., Hansen, A.M., and Trapp, S. (2006). Neuronal responses to transient hypoglycaemia in the dorsal vagal complex of the rat brainstem. *J. Physiol.* 570, 469–484.
- Bradley, C. (1988). Stress and diabetes. In *Handbook of Life Stress Cognition and Health*, S. Fisher and J. Reason, eds. (John Wiley & Sons), pp. 383–400.
- Capes, S.E., Hunt, D., Malmberg, K., and Gerstein, H.C. (2000). Stress hyperglycaemia and increased risk of death after myocardial infarction in patients with and without diabetes: a systematic overview. *Lancet* 355, 773–778.
- Dayas, C.V., Buller, K.M., Crane, J.W., Xu, Y., and Day, T.A. (2001). Stressor categorization: acute physical and psychological stressors elicit distinctive recruitment patterns in the amygdala and in medullary noradrenergic cell groups. *Eur. J. Neurosci.* 14, 1143–1152.
- Duan, D., Yue, Y., and Engelhardt, J.F. (2001). Expanding AAV packaging capacity with trans-splicing or overlapping vectors: a quantitative comparison. *Mol. Ther.* 4, 383–391.
- Dungan, K.M., Braithwaite, S.S., and Preiser, J.C. (2009). Stress hyperglycaemia. *Lancet* 373, 1798–1807.
- Ek, M., Kurosawa, M., Lundeberg, T., and Ericsson, A. (1998). Activation of vagal afferents after intravenous injection of interleukin-1 $\beta$ : role of endogenous prostaglandins. *J. Neurosci.* 18, 9471–9479.
- Ericsson, A., Kovács, K.J., and Sawchenko, P.E. (1994). A functional anatomical analysis of central pathways subserving the effects of interleukin-1 on stress-related neuroendocrine neurons. *J. Neurosci.* 14, 897–913.
- Garfield, A.S., Li, C., Madara, J.C., Shah, B.P., Webber, E., Steger, J.S., Campbell, J.N., Gavrilova, O., Lee, C.E., Olson, D.P., et al. (2015). A neural basis for melanocortin-4 receptor-regulated appetite. *Nat. Neurosci.* 18, 863–871.
- Gerfen, C.R., Paletzki, R., and Heintz, N. (2013). GENSAT BAC cre-recombinase driver lines to study the functional organization of cerebral cortical and basal ganglia circuits. *Neuron* 80, 1368–1383.
- Govorunova, E.G., Sineshchekov, O.A., Janz, R., Liu, X., and Spudich, J.L. (2015). NEUROSCIENCE. Natural light-gated anion channels: A family of microbial rhodopsins for advanced optogenetics. *Science* 349, 647–650.
- Gropp, E., Shanabrough, M., Borok, E., Xu, A.W., Janoschek, R., Buch, T., Plum, L., Balthasar, N., Hampel, B., Waisman, A., et al. (2005). Agouti-related peptide-expressing neurons are mandatory for feeding. *Nat. Neurosci.* 8, 1289–1291.
- Guyenet, P.G., Stornetta, R.L., Bochorishvili, G., Depuy, S.D., Burke, P.G., and Abbott, S.B. (2013). C1 neurons: the body's EMTs. *Am. J. Physiol. Regul. Integr. Comp. Physiol.* 305, R187–R204.
- Herman, J.P., and Cullinan, W.E. (1997). Neurocircuitry of stress: central control of the hypothalamo-pituitary-adrenocortical axis. *Trends Neurosci.* 20, 78–84.
- Hökfelt, T., Fuxe, K., Goldstein, M., and Johansson, O. (1973). Evidence for adrenaline neurons in the rat brain. *Acta Physiol. Scand.* 89, 286–288.
- Hu, F., Ren, J., Zhang, J.E., Zhong, W., and Luo, M. (2012). Natriuretic peptides block synaptic transmission by activating phosphodiesterase 2A and reducing presynaptic PKA activity. *Proc. Natl. Acad. Sci. USA* 109, 17681–17686.
- Kalsbeek, A., La Fleur, S., Van Heijningen, C., and Buijs, R.M. (2004). Suprachiasmatic GABAergic inputs to the paraventricular nucleus control plasma glucose concentrations in the rat via sympathetic innervation of the liver. *J. Neurosci.* 24, 7604–7613.
- Kfelt, T.H., Fuxe, K., Goldstein, M., and Johansson, O. (1974). Immunohistochemical evidence for the existence of adrenaline neurons in the rat brain. *Brain Res.* 66, 235–251.
- Krashes, M.J., Shah, B.P., Madara, J.C., Olson, D.P., Strohlic, D.E., Garfield, A.S., Vong, L., Pei, H., Watabe-Uchida, M., Uchida, N., et al. (2014). An excitatory paraventricular nucleus to AgRP neuron circuit that drives hunger. *Nature* 507, 238–242.
- Kvetnansky, R., Sabban, E.L., and Palkovits, M. (2009). Catecholaminergic systems in stress: structural and molecular genetic approaches. *Physiol. Rev.* 89, 535–606.
- Lamy, C.M., Sanno, H., Labouèbe, G., Picard, A., Magnan, C., Chatton, J.Y., and Thorens, B. (2014). Hypoglycemia-activated GLUT2 neurons of the nucleus tractus solitarius stimulate vagal activity and glucagon secretion. *Cell Metab.* 19, 527–538.
- Lang, C.H., Bagby, G.J., Nowotny, A., and Spitzer, J.J. (1985). Effects of toxic and nontoxic endotoxin derivatives on glucose kinetics. *Circ. Shock* 17, 301–311.
- Li, H.Y., Ericsson, A., and Sawchenko, P.E. (1996). Distinct mechanisms underlie activation of hypothalamic neurosecretory neurons and their medullary catecholaminergic afferents in categorically different stress paradigms. *Proc. Natl. Acad. Sci. USA* 93, 2359–2364.
- Liu, Z., Zhou, J., Li, Y., Hu, F., Lu, Y., Ma, M., Feng, Q., Zhang, J.E., Wang, D., Zeng, J., et al. (2014). Dorsal raphe neurons signal reward through 5-HT and glutamate. *Neuron* 81, 1360–1374.
- Luquet, S., Perez, F.A., Hnasko, T.S., and Palmiter, R.D. (2005). NPY/AgRP neurons are essential for feeding in adult mice but can be ablated in neonates. *Science* 310, 683–685.
- Madden, C.J., Stocker, S.D., and Sved, A.F. (2006). Attenuation of homeostatic responses to hypotension and glucoprivation after destruction of catecholaminergic rostral ventrolateral medulla neurons. *Am. J. Physiol. Regul. Integr. Comp. Physiol.* 291, R751–R759.
- Marik, P.E., and Bellomo, R. (2013). Stress hyperglycemia: an essential survival response! *Crit. Care Med.* 41, e93–e94.
- McCall, J.G., Al-Hasani, R., Siuda, E.R., Hong, D.Y., Norris, A.J., Ford, C.P., and Bruchas, M.R. (2015). CRH Engagement of the Locus Coeruleus Noradrenergic System Mediates Stress-Induced Anxiety. *Neuron* 87, 605–620.
- McCown, K.C., Malhotra, A., and Bistrian, B.R. (2001). Stress-induced hyperglycemia. *Crit. Care Clin.* 17, 107–124.
- Moore, R.Y., and Bloom, F.E. (1979). Central catecholamine neuron systems: anatomy and physiology of the norepinephrine and epinephrine systems. *Annu. Rev. Neurosci.* 2, 113–168.
- Morilak, D.A., Fornal, C.A., and Jacobs, B.L. (1987). Effects of physiological manipulations on locus coeruleus neuronal activity in freely moving cats. III. Glucoregulatory challenge. *Brain Res.* 422, 32–39.

- Morilak, D.A., Barrera, G., Echevarria, D.J., Garcia, A.S., Hernandez, A., Ma, S., and Petre, C.O. (2005). Role of brain norepinephrine in the behavioral response to stress. *Prog. Neuropsychopharmacol. Biol. Psychiatry* 29, 1214–1224.
- Morton, G.J., Cummings, D.E., Baskin, D.G., Barsh, G.S., and Schwartz, M.W. (2006). Central nervous system control of food intake and body weight. *Nature* 443, 289–295.
- Pacák, K., and Palkovits, M. (2001). Stressor specificity of central neuroendocrine responses: implications for stress-related disorders. *Endocr. Rev.* 22, 502–548.
- Paxinos, G., and Franklin, K.B.J. (2001). *The Mouse Brain in Stereotaxic Coordinates* (Academic Press).
- Rinaman, L. (2010). Ascending projections from the caudal visceral nucleus of the solitary tract to brain regions involved in food intake and energy expenditure. *Brain Res.* 1350, 18–34.
- Ritter, S., Bugarith, K., and Dinh, T.T. (2001). Immunotoxic destruction of distinct catecholamine subgroups produces selective impairment of glucoregulatory responses and neuronal activation. *J. Comp. Neurol.* 432, 197–216.
- Ritter, S., Dinh, T.T., and Li, A.J. (2006). Hindbrain catecholamine neurons control multiple glucoregulatory responses. *Physiol. Behav.* 89, 490–500.
- Ritter, S., Li, A.J., Wang, Q., and Dinh, T.T. (2011). Minireview: The value of looking backward: the essential role of the hindbrain in counterregulatory responses to glucose deficit. *Endocrinology* 152, 4019–4032.
- Sara, S.J. (2009). The locus coeruleus and noradrenergic modulation of cognition. *Nat. Rev. Neurosci.* 10, 211–223.
- Sawamoto, K., Nakao, N., Kobayashi, K., Matsushita, N., Takahashi, H., Kakishita, K., Yamamoto, A., Yoshizaki, T., Terashima, T., Murakami, F., et al. (2001). Visualization, direct isolation, and transplantation of midbrain dopaminergic neurons. *Proc. Natl. Acad. Sci. USA* 98, 6423–6428.
- Sawchenko, P.E., and Swanson, L.W. (1982). The organization of noradrenergic pathways from the brainstem to the paraventricular and supraoptic nuclei in the rat. *Brain Res.* 257, 275–325.
- Sawchenko, P.E., Li, H.Y., and Ericsson, A. (2000). Circuits and mechanisms governing hypothalamic responses to stress: a tale of two paradigms. *Prog. Brain Res.* 122, 61–78.
- Schreibofer, A.M., and Guyenet, P.G. (1997). Identification of C1 presynaptic neurons in rat rostral ventrolateral medulla by juxtacellular labeling in vivo. *J. Comp. Neurol.* 387, 524–536.
- Southwick, S.M., Krystal, J.H., Bremner, J.D., Morgan, C.A., 3rd, Nicolaou, A.L., Nagy, L.M., Johnson, D.R., Heninger, G.R., and Charney, D.S. (1997). Noradrenergic and serotonergic function in posttraumatic stress disorder. *Arch. Gen. Psychiatry* 54, 749–758.
- Stachniak, T.J., Ghosh, A., and Sternson, S.M. (2014). Chemogenetic synaptic silencing of neural circuits localizes a hypothalamus→midbrain pathway for feeding behavior. *Neuron* 82, 797–808.
- Stanford, S.C. (1995). Central noradrenergic neurones and stress. *Pharmacol. Ther.* 68, 297–342.
- Stotz-Potter, E.H., Willis, L.R., and DiMicco, J.A. (1996). Muscimol acts in dorsomedial but not paraventricular hypothalamic nucleus to suppress cardiovascular effects of stress. *J. Neurosci.* 16, 1173–1179.
- Sun, Y., Hunt, S., and Sah, P. (2015). Norepinephrine and Corticotropin-Releasing Hormone: Partners in the Neural Circuits that Underpin Stress and Anxiety. *Neuron* 87, 468–470.
- Taniguchi, H., He, M., Wu, P., Kim, S., Paik, R., Sugino, K., Kvitsiani, D., Fu, Y., Lu, J., Lin, Y., et al. (2011). A resource of Cre driver lines for genetic targeting of GABAergic neurons in cerebral cortex. *Neuron* 71, 995–1013.
- Tervo, D.G., Hwang, B.Y., Viswanathan, S., Gaj, T., Lavzin, M., Ritola, K.D., Lindo, S., Michael, S., Kuleshova, E., Ojala, D., et al. (2016). A Designer AAV Variant Permits Efficient Retrograde Access to Projection Neurons. *Neuron* 92, 372–382.
- Ulrich-Lai, Y.M., and Herman, J.P. (2009). Neural regulation of endocrine and autonomic stress responses. *Nat. Rev. Neurosci.* 10, 397–409.
- Ulrich-Lai, Y.M., and Ryan, K.K. (2014). Neuroendocrine circuits governing energy balance and stress regulation: functional overlap and therapeutic implications. *Cell Metab.* 19, 910–925.
- Verberne, A.J., and Sartor, D.M. (2010). Rostroventrolateral medullary neurons modulate glucose homeostasis in the rat. *Am. J. Physiol. Endocrinol. Metab.* 299, E802–E807.
- Vong, L., Ye, C., Yang, Z., Choi, B., Chua, S., Jr., and Lowell, B.B. (2011). Leptin action on GABAergic neurons prevents obesity and reduces inhibitory tone to POMC neurons. *Neuron* 71, 142–154.
- Wang, D., He, X., Zhao, Z., Feng, Q., Lin, R., Sun, Y., Ding, T., Xu, F., Luo, M., and Zhan, C. (2015). Whole-brain mapping of the direct inputs and axonal projections of POMC and AgRP neurons. *Front. Neuroanat.* 9, 40.
- Wickersham, I.R., Lyon, D.C., Barnard, R.J., Mori, T., Finke, S., Conzelmann, K.K., Young, J.A., and Callaway, E.M. (2007). Monosynaptic restriction of transsynaptic tracing from single, genetically targeted neurons. *Neuron* 53, 639–647.
- Wu, Z., Xu, Y., Zhu, Y., Sutton, A.K., Zhao, R., Lowell, B.B., Olson, D.P., and Tong, Q. (2012). An obligate role of oxytocin neurons in diet induced energy expenditure. *PLoS ONE* 7, e45167.
- Xiu, F., Stanojcic, M., Diao, L., and Jeschke, M.G. (2014). Stress hyperglycemia, insulin treatment, and innate immune cells. *Int. J. Endocrinol.* 2014, 486403.
- Yang, C.F., Chiang, M.C., Gray, D.C., Prabhakaran, M., Alvarado, M., Juntti, S.A., Unger, E.K., Wells, J.A., and Shah, N.M. (2013). Sexually dimorphic neurons in the ventromedial hypothalamus govern mating in both sexes and aggression in males. *Cell* 153, 896–909.
- Zhan, C., Zhou, J., Feng, Q., Zhang, J.E., Lin, S., Bao, J., Wu, P., and Luo, M. (2013). Acute and long-term suppression of feeding behavior by POMC neurons in the brainstem and hypothalamus, respectively. *J. Neurosci.* 33, 3624–3632.
- Zhang, J., Tan, L., Ren, Y., Liang, J., Lin, R., Feng, Q., Zhou, J., Hu, F., Ren, J., Wei, C., et al. (2016). Presynaptic Excitation via GABAB Receptors in Habenula Cholinergic Neurons Regulates Fear Memory Expression. *Cell* 166, 716–728.

**STAR★METHODS****KEY RESOURCES TABLE**

REAGENT or RESOURCE	SOURCE	IDENTIFIER
<b>Antibodies</b>		
Goat Anti-C-Fos	Santa Cruz	Cat# sc-52-G, RRID: AB_2629503
Rabbit Anti-C-Fos	Santa Cruz	Cat# sc-52, RRID: AB_2106783
Mouse Anti-oxytocin	Millipore	Cat# MAB5296, RRID: AB_2157626
Biotin-SP-conjugated Donkey anti-mouse	Jackson ImmunoResearch	Cat# 715-065-150, RRID:A B_2307438
Cy3-conjugated Streptavidin	Jackson ImmunoResearch	Cat# 016-160-084, RRID: AB_2337244
Rabbit Anti-vasopressin	Abcam	Cat# ab39363, RRID: AB_778778
Rabbit Anti-Tyrosine Hydroxylase	Millipore	Cat# AB152, RRID: AB_390204
Chicken Anti-GFP	Abcam	Cat# ab13970, RRID: AB_300798
Rabbit Anti-eGFP	Proteintech	Cat# 50430-2-AP, RRID: AB_11042881
Alexa Fluor 488-conjugated Goat Anti-Rabbit	Proteintech	Cat# SA00006-2, RRID: AB_2651036
Anti-Digoxigenin-POD	Roche	Cat# 11207733910, RRID: AB_514500
Alexa Fluor 488-conjugated Goat Anti-Chicken	ThermoFisher	Cat# A-11039, RRID: AB_142924
Alexa Fluor 488-conjugated Goat Anti-Rabbit	Jackson ImmunoResearch	Cat# 111-545-003, RRID: AB_2338046
Cy3-conjugated Goat Anti-Rabbit	Jackson ImmunoResearch	Cat# 111-165-008, RRID: AB_2338002
Cy2-conjugated Donkey Anti-Goat	Jackson ImmunoResearch	Cat# 705-225-147, RRID: AB_2307341
Alexa Fluor 647-conjugated Goat Anti-Rabbit	Jackson ImmunoResearch	Cat# 111-605-144, RRID: AB_2338078
<b>Bacterial and Virus Strains</b>		
AAV-flex-taCasp3-TEVp	Zhang et al., 2016, Dr. Minmin Luo	N/A
AAV-DIO-ChR2-mCherry	Liu et al., 2014, Dr. Minmin Luo	N/A
AAV-hM3Dq-2A-mCherry	Zhan et al., 2013, Dr. Minmin Luo	N/A
AAV-DIO-mCherry	Wang et al., 2015, Dr. Minmin Luo	N/A
AAV-DIO-mGFP	Wang et al., 2015, Dr. Minmin Luo	N/A
AAV-DIO-GCaMP3	This paper	N/A
AAV-EF1a-DIO-GtACR1-P2A-GFP-WPRE	This paper	N/A
rAAV2-CMV-retro-Cre-eGFP	Shanghai Taitool Bioscience	Catalog No. AAV2/2Retro-S0231
rAAV2-hSyn-retro-eGFP	Shanghai Taitool Bioscience	Catalog No. AAV2/2Retro-S0237
Rabies viruses SAD- $\Delta$ G-mCherry(EnvA)	BrainVTA, Wuhan	Catalog No. RV-306
AAV-DIO-TVA-EGFP	BrainVTA, Wuhan	Catalog No. AAV-903
AAV-DIO-G	BrainVTA, Wuhan	Catalog No. AAV-902
<b>Chemicals, Peptides, and Recombinant Proteins</b>		
Clozapine N-oxide	Enzo	Catalog No. BML-NS105-0025, Lot#05041525
Lipopolysaccharides	Sigma	Catalog No. L2880; Lot#046M4045V
Trizol	Life Technologies	Catalog No. 15596-026
4-Aminopyridine	Tocris	Catalog No. 0940
Tetrodotoxin	Tocris	Catalog No. 1078
Acetylcholine	Sigma	Catalog No. A6625
Dextran, Texas Red, 3000MW, Lysine fixable	ThermoFisher	Catalog No. D3328; Lot#1540675
Alexa Fluor 488-conjugated Cholera Toxin Subunit B	ThermoFisher	Catalog No. C22841; Lot#1696218
DNQX	Sigma	Catalog No. D0540
<b>Critical Commercial Assays</b>		
Corticosterone ELSA kits	ENZO Life Science	Cat# ADI-900-097, RRID: AB_2307314
Epinephrine ELSA kits	Abnova	Catalog No. KA3837; Lot#151032

(Continued on next page)

**Continued**

REAGENT or RESOURCE	SOURCE	IDENTIFIER
PrimeScript RT Master Mix	Takara	Catalog No. RR036A
TSA Plus Cyanine 5	PerkinElmer	Catalog No. NEL745B001KT
Experimental Models: Organisms/Strains		
Mouse / C57BL/6J	Keaoxieli Animal Feed	N/A
Mouse / <i>Dbh-Cre</i>	MMRRC	RRID: MMRRC_036734-UCD
Mouse / <i>Slc17a6-ires-Cre</i>	Jackson laboratory	Stock# 016963; RRID: IMSR_JAX: 016963
Mouse / <i>Crh-ires-Cre</i>	Jackson laboratory	RRID: IMSR_JAX:012704
Mouse / <i>Oxytocin-ires-Cre</i>	Jackson laboratory	RRID: IMSR_JAX:024234
Mouse / <i>Th-GFP</i>	<a href="#">Sawamoto et al., 2001</a> , Dr. K. Kobayashi	RRID: IMSR_RBRC03162
Software and Algorithms		
Graphpad prism 6	GraphPad Software	N/A
Imaris	Bitplane	N/A
ImageJ	NIH	<a href="https://imagej.nih.gov/ij/">https://imagej.nih.gov/ij/</a>
Excel	Microsoft	N/A
Other		
optical fiber	Thorlabs	FT200UMT
473nm blue laser	Dreamlaser, Shanghai	SDL-473-100T

**CONTACT FOR REAGENT AND RESOURCE SHARING**

Further information and requests for resources and reagents may be directed to and will be fulfilled by the Lead Contact, Cheng Zhan ([zhancheng@nibs.ac.cn](mailto:zhancheng@nibs.ac.cn)).

**EXPERIMENTAL MODEL AND SUBJECT DETAILS**

The care and use of animals in the course of this study conformed to the institutional guidelines of the National Institute of Biological Sciences, Beijing, as well as governmental regulations. Mice were singly housed under controlled temperature (22–25°C) and photo-period (12/12 light/dark; light from 9 pm to 9 am), were fed a standard chow diet (SPF Rodent Feed; 4% fat; Keaoxieli Animal Feed, China), and were offered ad libitum water. All experiments were performed on adult mice (10–16 weeks old, both male and female). For all stress challenge experiments, only male mice were used. Behavior experiments were performed from 10am-2 pm.

The mouse strains used included *Dbh-Cre*, *Slc17a6-ires-Cre*, *Crh-ires-Cre*, *Oxytocin-ires-Cre*, *Th-GFP*, and wide-type C57BL/6J mice. The *Dbh-Cre* (MMRRC strain Name STOCK Tg(*Dbh-cre*)KH212Gsat/Mmc<sup>d</sup>) mouse line was produced by Dr. Nathaniel Heintz (The Rockefeller University) and Dr. Charles Gerfen (National Institutes of Health) laboratories using the BAC-transgenic strategy ([Gerfen et al., 2013](#)). The *Slc17a6-ires-Cre* (Jackson Laboratory stock No: 016963) mouse line was produced by Dr. Bradford B. Lowell's laboratory (Harvard Medical School) ([Yang et al., 2013](#)). The *Crh-ires-Cre* (Jackson Laboratory stock No: 012704) mouse line was produced by Dr. Josh Huang's laboratory (Cold Spring Harbor laboratory) ([Taniguchi et al., 2011](#)). The *Oxt-ires-Cre* (Jackson Laboratory stock No: 024234) mouse line was produced by Dr. David P Olson's laboratory (University of Michigan Medical School) ([Wu et al., 2012](#)). The *Th-GFP* transgenic mice was produced by Dr. Hideyuki Okano (Keio University School of Medicine) ([Sawamoto et al., 2001](#)). We generated *Slc17a6-Cre::Th-GFP* mice by crossing *Slc17a6-Cre* and *Th-GFP* mouse lines.

**METHOD DETAILS****Production of viral vectors**

The AAV-flex-taCasp3-TEVp vector was a gift from Drs. Nirao Shah & Jim Wells of UCSF (Addgene plasmid # 45580). The AAV-DIO-ChR2-mCherry construct was a gift from Dr. Karl Deisseroth of Stanford University. The coding sequence of hM3Dq-2A-mCherry was inserted into an AAV-DIO vector with a CMV early enhancer/chicken β-actin (CAG) promoter. AAV-DIO-mGFP and AAV-DIO-GCaMP3 were constructed by replacing the coding region of hChR2 (H134R)-EYFP with the coding sequence of the membrane GFP (mGFP, Addgene plasmid 14757), or with GCaMP3 in the AAV-EF1a-DIO-hChR2 (H134R)-EYFP-WPRE-HGHpA plasmid (Addgene plasmid 20298). The sequence of *Guillardia theta* anion channel rhodopsins 1 (GtACR1) was synthesized according to the original paper ([Govorunova et al., 2015](#)). AAV-EF1a-DIO-GtACR1-P2A-GFP-WPRE was constructed by ligating GtACR1 and eGFP with a DNA fragment encoding P2A peptide and inserting into AAV-EF1a-DIO backbone in an inverted orientation. All coding sequences

were in a 3' to 5' orientation relative to the promoter. All AAV vectors were packaged into 2/9 serotypes in the laboratory of Dr. Minmin Luo (NIBS, Beijing) with the assistance of Dr. Dong Duan (University of Missouri) (Duan et al., 2001). Final viral vector titers were  $>10^9$  particles/ $\mu$ l.

The initial rabies viruses SAD- $\Delta$ G-mCherry(EnvA) and the cell line were kindly provided by Dr. Edward M. Callaway (Salk Institute). The rabies viruses and the other two helper virus were produced and concentrated commercially by BrainVTA of Wuhan, China.

### Stereotaxic virus and tracer injections

Mice were anesthetized with pentobarbital (80 mg/kg; IP) and placed in a temperature-controlled stereotaxic holder. A small hole was opened in the skull. Pulled glass pipettes ( $\sim$ 20  $\mu$ m tip diameter) were filled with virus and inserted into the target areas. Viral vectors were injected into the brain under pressure (infusion speed = 23 nl/minute) (Nanoliter 2000 Injector, WPI). To selectively kill particular subpopulations of catecholaminergic (CA) neurons, a Cre-dependent AAV-flex-taCasp3-TEVp vector (800-1000 nl) was bilaterally infused into the LC (coordinate AP/DV/ML:  $-5.5/-2.6/\pm 1.0$  mm), NTS, or VLM of *Dbh-Cre* mice (named *Dbh-LC*<sup>Casp3</sup>, *Dbh-NTS*<sup>Casp3</sup>, or *Dbh-VLM*<sup>Casp3</sup> mice respectively). In order to ablate the entire NTS or VLM CA population, AAV-flex-taCasp3-TEVp was injected into the rostral and caudal parts of both the NTS and VLM (NTS coordinate AP/DV/ML:  $-8.0/-3.1/0$  mm and  $-7.2/-3.3/\pm 0.5$  mm; VLM coordinate AP/DV/ML:  $-6.6/-4.3/\pm 1.3$  mm and  $-7.5/-4.2/\pm 1.3$  mm). For the chemogenetic activation of particular populations of CA neurons, AAV-DIO-hM3Dq-mCherry (800-1000 nl) was bilaterally injected into the LC, NTS, or VLM of *Dbh-Cre* mice (named *Dbh-LC*<sup>hM3Dq</sup>, *Dbh-NTS*<sup>hM3Dq</sup>, or *Dbh-VLM*<sup>hM3Dq</sup> mice respectively). AAV-DIO-mCherry was used as a control to generate *Dbh-LC*<sup>mCherry</sup>, *Dbh-NTS*<sup>mCherry</sup>, and *Dbh-VLM*<sup>mCherry</sup> mice. For calcium imaging, AAV-DIO-hM3Dq-mCherry and AAV-DIO-GCaMP3 were mixed in equal volumes prior to viral injections.

For cell-type-specific anterograde tracing, a viral tracer, AAV-DIO-mGFP (300 nl), was injected into the VLM of *DBH-Cre* mice. For retrograde tracing, tract tracers (0.1% Alexa Fluor 488 conjugated Cholera Toxin Subunit B, CTb-488, Catalog No. C34775; 5% Texas Red conjugated dextran amine, TRDA, MW = 3 KD, TR3K, Catalog No. D3328; ThermoFisher) were unilaterally injected into the PVN or the spinal cord (coordinate AP/DV/ML: T8-T11/ $-0.5/\pm 0.3$  mm). Post-surgery, mice were caged individually and allowed to recover for at least 2 weeks before any studies were performed.

The modified rabies virus based three-virus system was used for mapping the whole-brain inputs to VLM CA neurons (Wickersham et al., 2007). Equal volumes of AAV-DIO-TVA-EGFP and AAV-DIO-G were mixed and then  $\sim$ 200 nL of the AAV mixture was unilaterally injected into the VLM of *Dbh-Cre* mice. Two weeks later, the rabies virus SAD- $\Delta$ G-mCherry(EnvA) (300 nl), which lacks the rabies glycoprotein (G) gene and was pseudotyped with the avian sarcoma leucosis virus envelope protein (EnvA), was injected into the same location in a biosafety level-2 lab facility (Figures S6A and S6B). Starter neurons were characterized by the coexpression of RV-mCherry and TVA-EGFP, which were restricted in the VLM (Figure S6C). Following one week of viral replication and *trans*-synaptic spread, mouse brains were prepared for further analysis.

For selectively stimulating spinally-projecting RVLM CA neurons, rAAV2-CMV-retro-Cre-eGFP (Taitool, Shanghai) was injected into the spinal cord (T8-T11), and AAV-DIO-ChR2-mCherry was injected into the RVLM.

### Glucose, corticosterone, and epinephrine measurement

To measure blood glucose, the ends of mouse tails were cut horizontally with a razor blade and a small drop of blood was collected with gentle massage. Glucose levels were then measured using a blood glucose meter (One touch, Johnson & Johnson Medical). Basal blood glucose levels were first measured at the onset of the dark phase of the photoperiod. Following stress treatments or injections of CNO (Catalog No. BML-NS105-0025, Enzo, 1 mg/kg bodyweight in saline, IP), LPS (Catalog No. L2880, Sigma, 10 ug /kg bodyweight in saline, IP), or saline, blood glucose levels were measured at various time points. No food was supplied during the blood glucose measurement period.

For serum assays, 60 min after the injection of LPS, CNO, or saline, blood was drawn from the retrobulbar intraorbital capillary plexus, and serum was then separated by centrifugation (13,000 rpm for 15 min). Commercial ELISA kits were used for measuring serum corticosterone (Catalog No. ADI-900-097, ENZO Life Science) and epinephrine (Catalog No. KA3837, Abnova) levels. Glucose, corticosterone, and epinephrine measurements were independently replicated by two testers.

### Real-time PCR

Animals were deeply anesthetized 90 min following the injection of CNO or saline. Livers were rapidly dissected and stored in liquid nitrogen. Total RNA was extracted using Trizol reagent (Catalog No. 15596-026, Life Technologies). Total RNA (1  $\mu$ g) was reverse transcribed into cDNA using PrimeScript RT Master Mix (Perfect Real Time, Catalog No. RR036A, Takara). Gene expression levels were then analyzed using a BioRad CFX96 real-time PCR detection system (Bio-Rad Laboratories) and the expression levels of target genes were normalized to *Gapdh* RNA expression.

### Optogenetic experiments

For optogenetic experiments, a small craniotomy was made in the skull. AAV-DIO-ChR2-mCherry vectors (1000 nl) or AAV-DIO-GtACR1-GFP vectors (1000 nl) were bilaterally delivered into target areas, and then an optical fiber (200  $\mu$ m in diameter, NA = 0.39) was inserted into same locations and affixed to the skull with dental cement. For optogenetic activation, blue laser pulses (473 nm wavelength, 5 ms pulse duration, 20 Hz frequency, 1 s on and 1 s off; 20 mw continuous output power measured at the fiber

tip) were used. For optogenetic inhibition, blue laser pulses (473 nm wavelength, 3 s on and 3 s off; 5 mw continuous output power measured at the fiber tip) were used.

### Adrenalectomy and spinal transection

Anesthetized mice were placed in ventral recumbency and a ~2 cm long midline incision was made just caudal to the peak of the animal's dorsal hump. Forceps were inserted through the incision and used to remove the adrenal glands bilaterally. Post-surgery, 0.9% saline solution was administered in place of drinking water.

For spinal transection, a longitudinal incision ~4 cm long was made above the spinal cord. Hemostats or forceps were used to detach muscle from bone on the spinal laminae. After exposing vertebral column T4-T6, the spinal cord was completely cross-sectionally transected using venus scissors at the T5 level. Body weights and basal blood glucose levels were monitored, and mice whose weight or glucose levels have declined by more than 20% were excluded from any subsequent experiments.

### Electrophysiological Recordings and Calcium Imaging

Slice preparation, physiological recordings, photostimulation, and drug applications were performed as described previously (Hu et al., 2012; Zhang et al., 2016). Briefly, neurons were recorded from slices (300  $\mu$ m) that were submerged and superfused with oxygenated artificial cerebrospinal fluid (aCSF) (29–30°C) containing 125 mM NaCl, 2 mM CaCl<sub>2</sub>, 2.5 mM KCl, 1.3 mM MgCl<sub>2</sub>, 1.3 mM NaH<sub>2</sub>PO<sub>4</sub>, 1.3 mM Na-ascorbate, 0.6 mM Na-pyruvate, 25 mM NaHCO<sub>3</sub>, and 20 mM glucose. Recording pipettes (3–5 M $\Omega$ ) were pulled with a micropipette puller (P97, Sutter Instruments). For whole-cell patch and cell-attached recordings, neurons in the VLM were identified by fluorescent signals and DIC observation under an upright microscope. The traces were low-pass filtered at 2.6 kHz and digitized at 10 kHz (DigiData1322A, Molecular Devices). A minimum of 5 min of base line was collected from each cell. For optogenetic stimulation, generation of light pulses (5 ms in duration, and 5, 10, 20, or 50 Hz frequency) was controlled by digital commands from Digidata 1322A data acquisition system. The data were analyzed using Clampfit 10 software (Molecular Devices). For drug application, DNQX (10  $\mu$ M, Sigma), TTX, tetrodotoxin (10  $\mu$ M, Tocris), and 4-AP, 4-Aminopyridine (1 mM, Tocris) were added into the superfusion medium. CNO (30  $\mu$ M) and acetylcholine (10  $\mu$ M) were delivered to the imaged area under pressure using an 8-channel drug delivery system (MPS-1, Inbio Life Science Instrument).

Calcium imaging of brain slices was performed under an upright confocal microscope (FV1000, Olympus) and time-lapse images were captured at 1 frame/sec. Data are presented as the relative change in fluorescence ( $\Delta F/F$ ). CNO perfusion resulted in Ca<sup>2+</sup> transients in hM3Dq/mCherry-expressing neurons (Figure S2A). Perfusion of CNO did not increase Ca<sup>2+</sup> signals in the mCherry-only expressing neurons of control brain slices and IP injection of CNO did not elicit Fos signals in control mice (*Dbh*-VLM<sup>mCherry</sup> mice) (Figures S2C–S2E).

### Histology and immunoassaying

For Fos immunostaining, mice received an electrical footshock, 1 hr restraint in a tapered plastic film, or an injection of CNO, LPS, or saline (IP), and were deeply anaesthetized 90 min later. Animals were then perfused intracardially with cold saline solution, followed by 4% paraformaldehyde in PBS with 0.2% picric acid. Brains were extracted and post-fixed in 4% paraformaldehyde overnight at 4°C and cryoprotected with 30% sucrose. Coronal sections (40–50  $\mu$ m) were cut with a freezing cryostat (Leica CR 1900) and mounted on glass slides. Brain sections were incubated with primary antibodies against Fos (rabbit, 1:1000, RRID: AB\_2106783, Santa Cruz), Oxt (1:500, RRID: AB\_2157626, Millipore), AVP (1:500, RRID: AB\_778778, Abcam), or TH (rabbit, 1:1000, RRID: AB\_390204, Millipore) overnight at 4°C, and then incubated with Cy2-, Cy3-, or Alexa 647-conjugated secondary antibodies (1:1000, Jackson ImmunoResearch) at room temperature for 3 hr. Fluorescence images were acquired using a confocal microscope (DigitalEclipse A1, Nikon) or an automated slider scanner (VS120 virtual Slide, Olympus), and processed using ImageJ (NIH).

In the monosynaptic tracing experiments, whole-brain sections were imaged using a VS120 scanner. The locations of labeled neurons and outlines of the brain regions were manually defined according the mouse brain atlas (Paxinos and Franklin, 2001). Cell numbers were counted automatically using commercial Imaris software (Bitplane).

### RNA in situ hybridization

Mice with unilateral injections of rAAV2-hSyn-retro-eGFP (Taitool) into the VLM were perfused with 0.01M DEPC treated PBS (DEPC-PBS), followed by 4% paraformaldehyde in DEPC-PBS. Brains were extracted and post-fixed overnight at 4°C, then cryoprotected with 30% sucrose. Then brain sections (50  $\mu$ m) were analyzed by *in situ* hybridization as previously described (Xiu et al., 2014). Briefly, brain sections were rinsed with DEPC-PBS, then permeabilized with DEPC-PTW (DEPC-PBS, 0.1%Tween20) and 0.5% Triton 2 × SSC. After incubation for 2 h in prehybridization buffer (50% formamide, 5 × SSC, 5mM EDTA pH8.0, 0.1% Tween20, 1% CHAPS), brain sections were hybridized with a digoxigenin labeled *Trh* antisense cRNA probe (NCBI Accession number NM\_009426.1) for 20 h at 65°C in hybridization solution (50% formamide, 5 × SSC, 5 mM EDTA pH8.0, 0.1%Tween20, 1%CHAPS, 300  $\mu$ g/ml tRNA, 1 × Denholt's solution, 1% Heparin). After hybridization, brain sections were incubated with Anti-Digoxigenin-POD (1:500, RRID: AB\_514500, Roche) at 4°C for 30h. TSA Plus Cyanine 5 (1:100, NEL745B001KT, PerkinElmer) was used to detect the primary antibody. To enhance the GFP signal in PVN neurons labeled by rAAV2-hSyn-retro-eGFP, brain sections were incubated with primary rabbit antibody against GFP (1:500, RRID: AB\_11042881, Proteintech), and then incubated with Alexa 488 goat anti-rabbit secondary antibody (1:500, RRID: AB\_2651036, Proteintech).

## QUANTIFICATION AND STATISTICAL ANALYSIS

All quantifications were performed not blinded. Statistical analyses were performed using Graphpad prism 6 and Excel. Statistical details including the definitions and exact value of n (e.g., number of animals, number of neurons, etc), deviations, p values, and the types of the statistical tests can be found in the Figures and Figure Legends. All statistical comparisons were conducted on data originating from two or more biologically independent experimental replicates. All data are shown as means  $\pm$  SEM. Two group comparisons were analyzed using two-tailed Student's t test. Comparisons between groups with two or more factors were analyzed using two-way ANOVA, followed by Bonferroni's post hoc test.  $p < 0.05$  was considered significant. \* indicates  $p < 0.05$ , \*\*  $p < 0.01$ , and \*\*\*  $p < 0.001$ , \*\*\*\*  $p < 0.0001$ . Correlations were computed using Pearson's correlation coefficient.

Further requests for data used in this study can be directed to the corresponding author.

**Supplemental Information**

**A Central Catecholaminergic Circuit Controls**

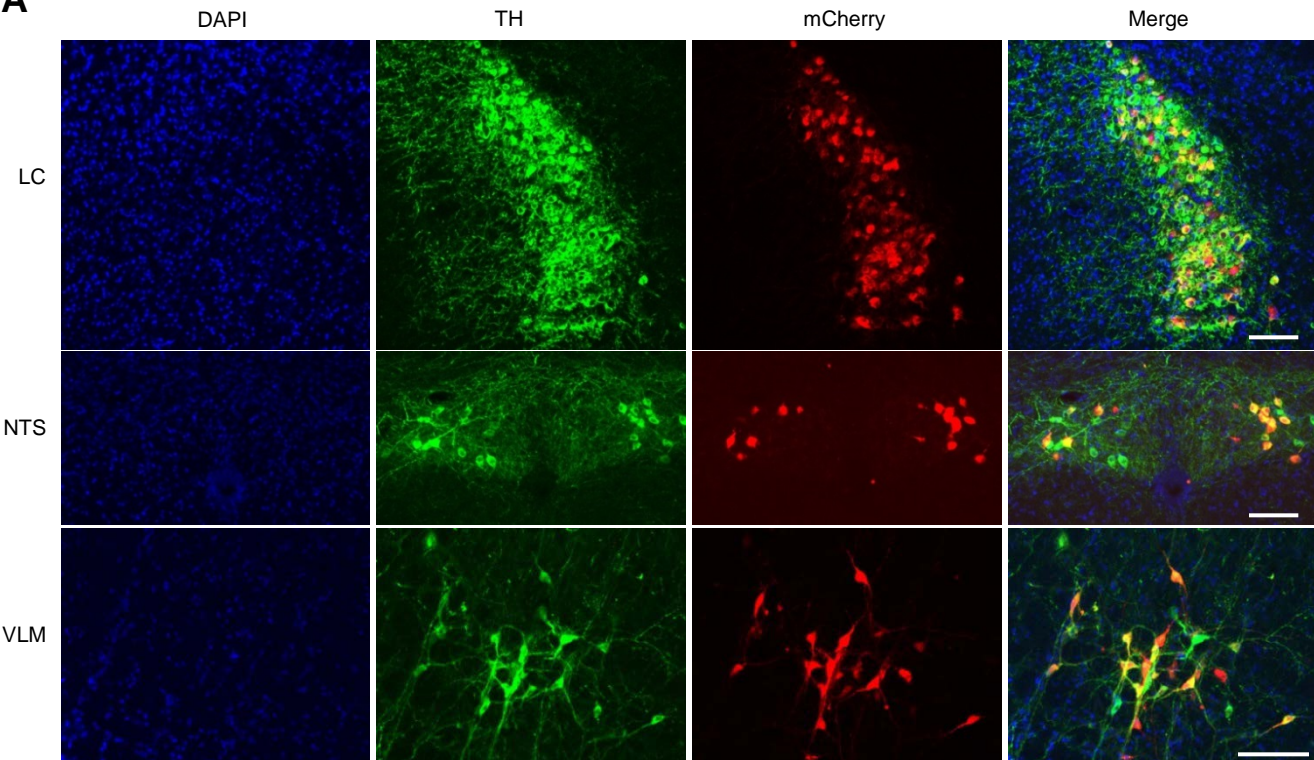
**Blood Glucose Levels during Stress**

**Zhe Zhao, Liang Wang, Wenling Gao, Fei Hu, Juen Zhang, Yuqi Ren, Rui Lin, Qiru Feng, Mingxiu Cheng, Dapeng Ju, Qingsheng Chi, Dehua Wang, Sen Song, Minmin Luo, and Cheng Zhan**

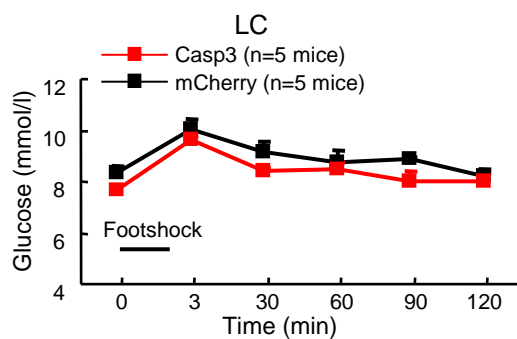
# Supplemental Figures

Figure S1

A



B



C

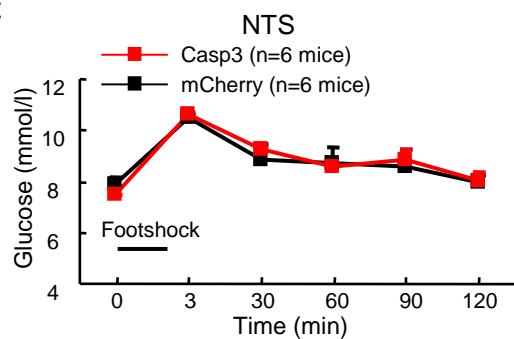


**Figure S1, related to Figure 1. CA neurons in the LC or NTS have no significant effect on footshock-induced hyperglycemia.**

**A)** AAV-DIO-mCherry was injected into the LC, NTS, or VLM of *Dbh-Cre* mice to generate *Dbh-LC<sup>mCherry</sup>*, *Dbh-NTS<sup>mCherry</sup>*, and *Dbh-VLM<sup>mCherry</sup>* control animals. mCherry (red) was selectively expressed in TH-expressing neurons (green) within the LC (top panel), NTS (middle panel), or VLM (bottom panel). Scale bar: 100  $\mu$ m.

**B-C)** Ablation of CA neurons in the LC (B) or NTS (C) did not affect footshock-induced hyperglycemia. Two-way ANOVA analyses followed by Bonferroni's post hoc test.

**Figure S2**

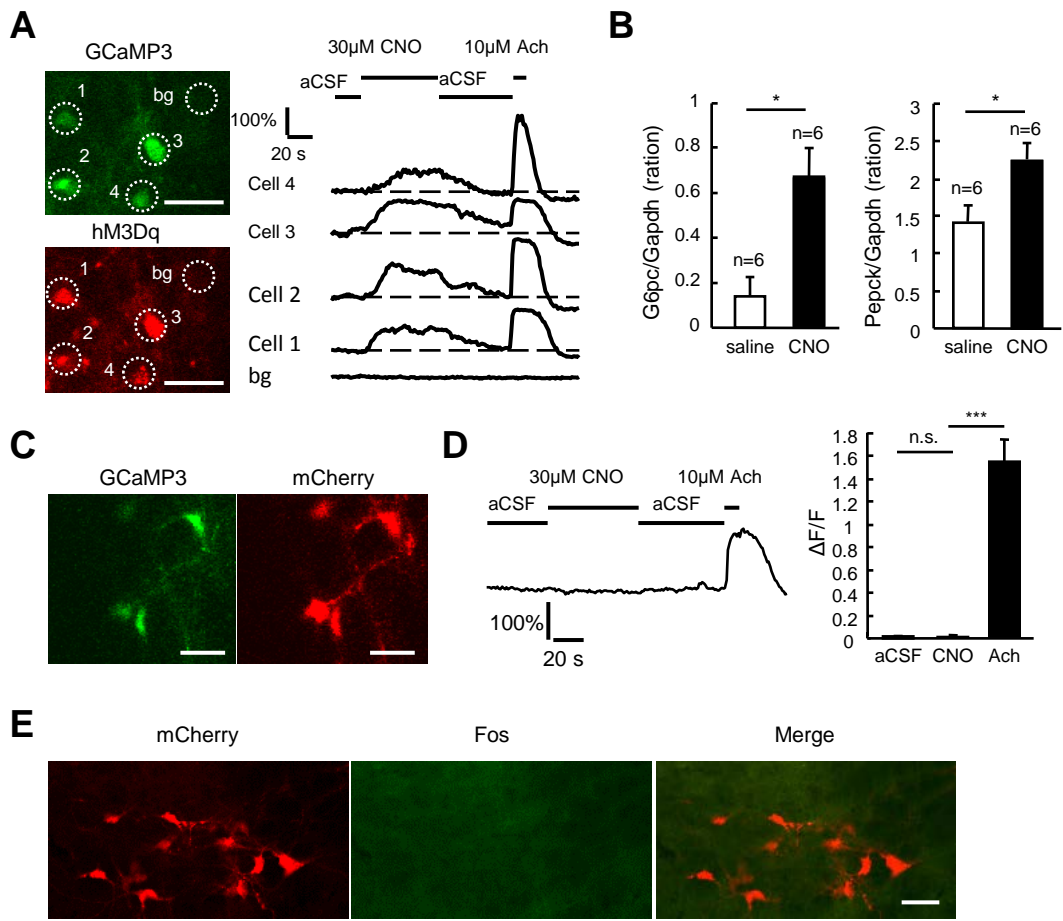


**Figure S2, related to Figure 4. Selective activation of VLM CA neurons using the DREADD method.**

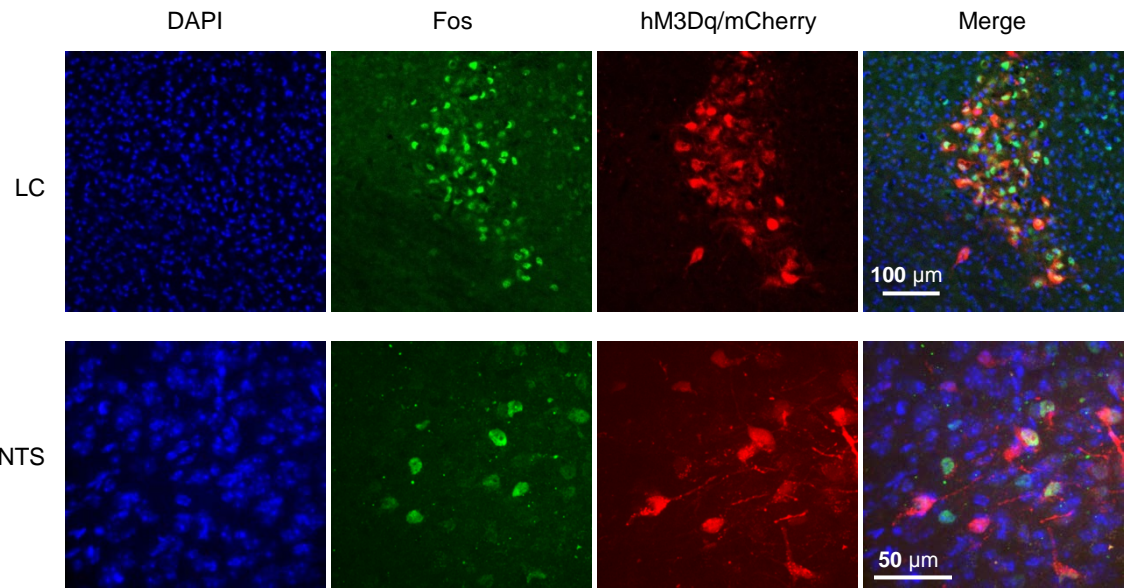
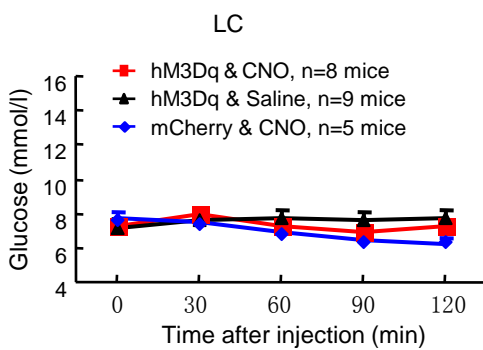
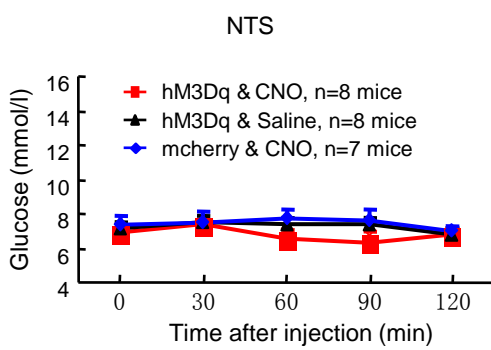
**A)** Following the coexpression of the calcium indicator GCaMP3 (green) and hM3Dq/mCherry (red) in VLM CA neurons (left column), calcium imaging experiments in brain slices revealed that both CNO and acetylcholine (ACh, a positive control) produced calcium transients in these neurons (white circle marked, middle column). bg, background. Calcium signals:  $\Delta F/F = 0.73 \pm 0.05$ ,  $n = 21$  neurons from 3 mice. Scale bar: 50  $\mu$ m.

**B)** Injection of CNO increased mRNA levels of hepatic *G6pc* (left panel) and *Pepck* (right panel) in *Dbh-VLM<sup>hM3Dq</sup>* mice. \*  $p < 0.05$ ; Student's t-test between groups.

**C)** Coexpression of GCaMP3 (green) and mCherry (red) in VLM CA neurons. Scale bar: 50  $\mu$ m.

**D)** A representative raw trace shows that ACh, but neither CNO nor aCSF (negative control), produced calcium transients in a VLM CA neuron of a *Dbh-VLM<sup>mCherry</sup>* mouse (left). Right panel shows group data ( $n = 19$  neurons from 3 mice). n.s., not significant; \*\*\*  $p < 0.001$ ; Paired Student's t-test.

**E)** CNO injections did not elicit Fos expression (green) in VLM CA neurons (red) in *Dbh-VLM<sup>mCherry</sup>* mice. Zero Fos positive neurons in  $991 \pm 218$  mCherry-labeled VLM CA neurons ( $n = 4$  mice). Scale bar: 50  $\mu$ m.

**Figure S3****A****B****C****Figure S3, related to Figure 4. Selective activation of neither LC nor NTS CA neurons increased blood glucose levels.**

**A)** Following the expression of hM3Dq/mCherry in LC (top panel) or NTS (bottom panel) CA neurons, the injection of CNO (IP injection) elicited Fos expression (green) in hM3Dq<sup>+</sup> neurons (red).

**B-C)** Injection of CNO into *Dbh-LC<sup>hM3Dq</sup>* (B) and *Dbh-NTS<sup>hM3Dq</sup>* (C) mice did not increase blood glucose levels. There was no significant difference between the three groups in blood glucose levels at any of the different time points. Two-way ANOVA followed by Bonferroni's post hoc test. For the LC: animal groups  $F(2,19) = 1.147$ ,  $p = 0.338$ ; For the NTS: animal groups  $F(2,20) = 3.295$ ,  $p = 0.062$ .

**Figure S4**

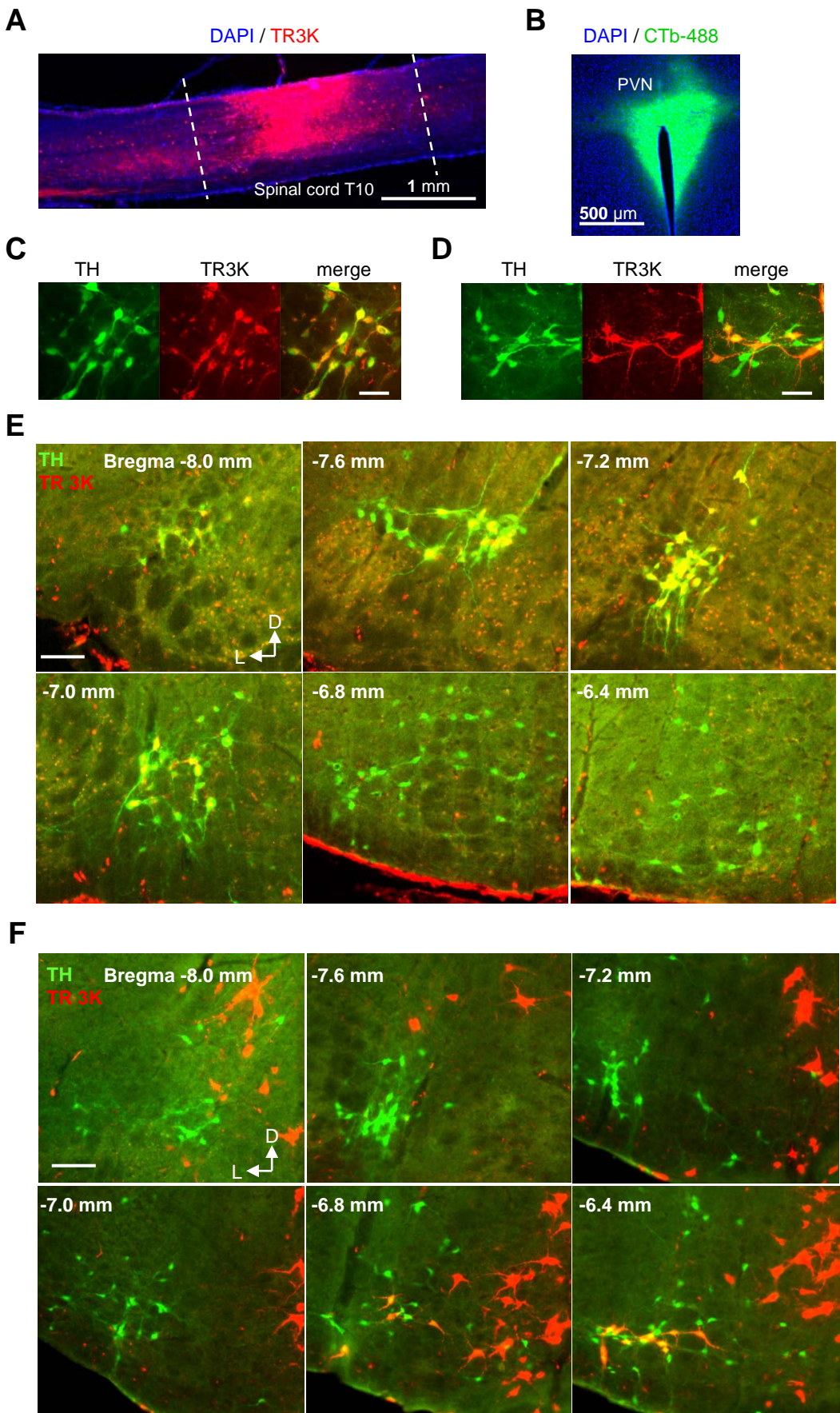


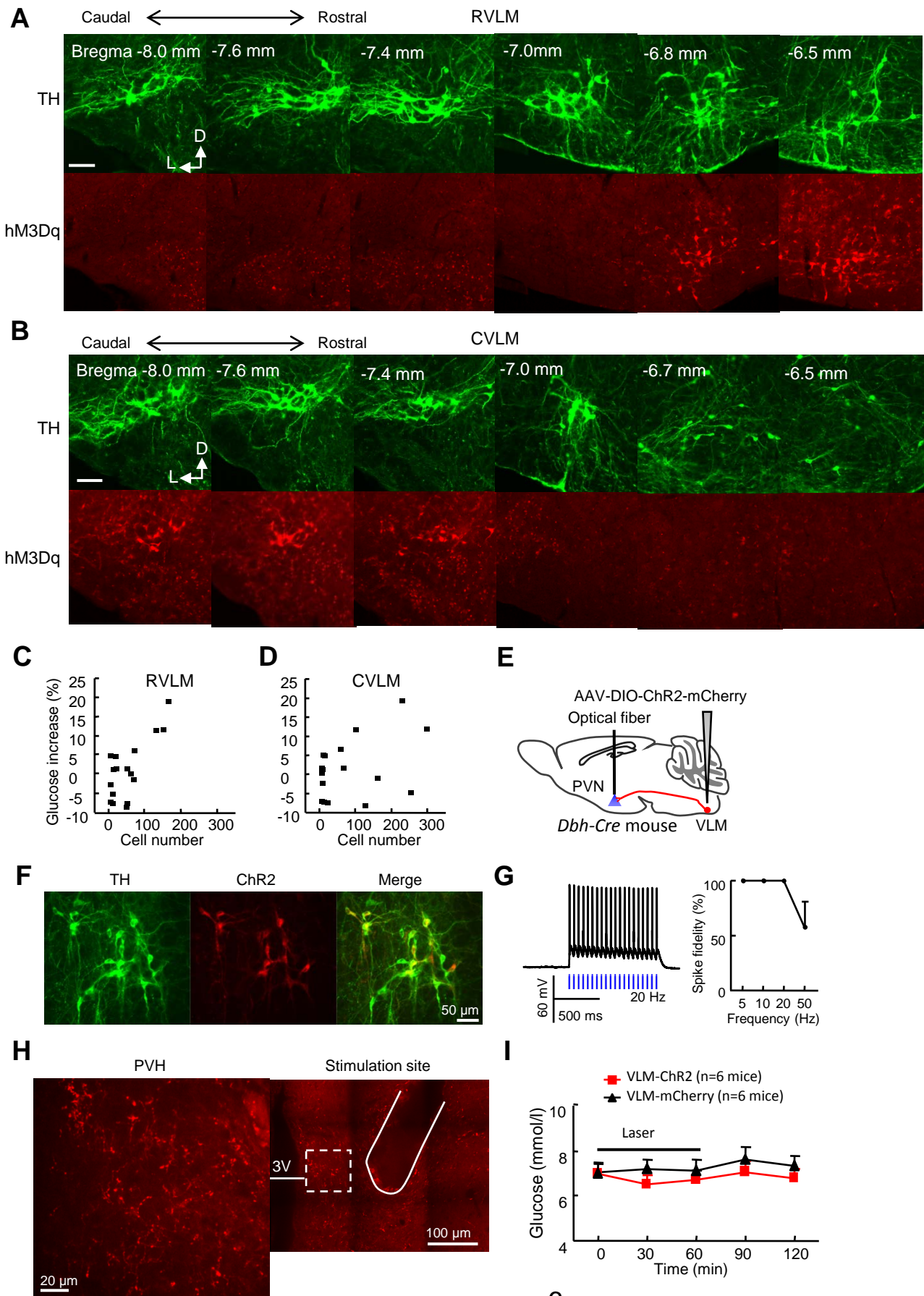
**Figure S4, related to Figure 5. Retrograde labeling of PVN- and spinally-projecting VLM CA neurons.**

**A-B)** Sites of injections of TR3K (red) into the spinal cord T10 (A) and CTb-488 (green) into the PVN (B).

**C-D)** Representative images showing TR3K (red) retrograde-labeled PVN-projecting (C) and spinally-projecting (D) TH-immunoreactive neurons (green) in the VLM. Scale bar: 40 µm.

**E)** Series of coronal sections showing the pattern of TR3K (red) retrograde-labeled TH-immunoreactive neurons (green) in the VLM following TR3k injection into the PVN. Scale bar: 100 µm. D: dorsal, L: lateral.

**F)** Series of coronal sections showing the pattern of TR3K (red) retrograde-labeled TH-immunoreactive neurons (green) in the VLM following TR3k injection into the spinal cord. Scale bar: 100 µm. D: dorsal, L: lateral.

**Figure S5**

**Figure S5, related to Figure 5. CA neurons in the RVLM, but not CVLM, play key roles in mediating stress-induced hyperglycemia.**

**A)** Series of coronal sections showing the pattern of hM3Dq/mCherry-labeled (red, bottom panels) TH-immunoreactive neurons (green, top panels) in the VLM following AAV-DIO-hM3Dq injection into the RVLM of a *Dbh-Cre* mouse. D: dorsal, L: lateral. Scale bar: 100  $\mu$ m.

**B)** Series of coronal sections showing the pattern of hM3Dq/mCherry-labeled (red, bottom panels) TH-immunoreactive neurons (green, top panels) in the VLM following AAV-DIO-hM3Dq injection into the CVLM of a *Dbh-Cre* mouse. Scale bar: 100  $\mu$ m.

**C-D)** The increase of blood glucose in *Dbh-VLM<sup>Casp3</sup>* mice following LPS challenge is positively correlated with the surviving cell number of CA neurons in the RVLM (C) but not in the CVLM (D). Each square represents data from a single mouse.

E-H) Optogenetic activation of the VLM-PVN circuit. (E) Cartoon of a terminal stimulation experiment in the PVN of *Dbh-Cre* mice. Two weeks after the viral injection, ChR2-mCherry (red) was selectively expressed in VLM CA neurons (green) (F). Whole-cell patch recordings showing that blue light (5-ms duration, 20 Hz) evoked stable firing of action potentials from a representative VLM CA neuron expressing ChR2-mCherry (G, left panel). Firing of VLM CA neurons was faithfully triggered by light pulses up to 20 Hz, but not 50 Hz (right panel,  $n = 4$  neurons) (G, right panel). (H) ChR2/mCherry-expressing CA axonal projections and optical fiber placement (white solid line) in the PVN of a *Dbh-VLM<sup>ChR2</sup>* mouse. The left panel is a zoomed-in view of the boxed region (white dotted line) in the PVN.

**I)** Light stimulation (1 second on, 1 second off, 5-ms duration, 20 Hz for 1 hour, horizontal bar) of VLM-derived CA nerve endings in the PVN of *Dbh-VLM<sup>ChR2</sup>* mice did not increase blood glucose levels. Two-way ANOVA analyses followed by Bonferroni's post hoc test between *Dbh-VLM<sup>ChR2</sup>* and *Dbh-VLM<sup>mCherry</sup>* mice: animal groups F(1,10) = 0.965, p = 0.349; time F(4,40) = 0.955, p = 0.442; interaction between time and animal groups F(4,40) = 0.429, p = 0.786.

## Figure S6

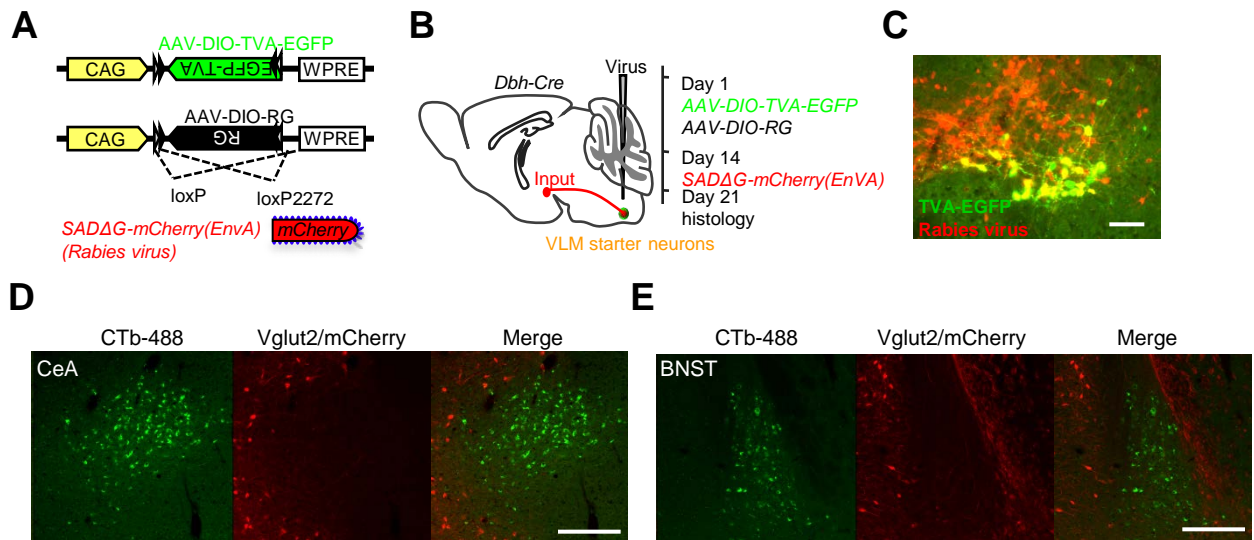


**Figure S6, related to Figure 6. Identification of direct inputs to VLM CA neurons using stereotaxic injection of the modified rabies virus into *Dbh-Cre* mice.**

**A-B)** Cartoons illustrating the experimental design (B) of trans-synaptic retrograde labeling by employing the Cre-dependent modified rabies virus (A).

**C)** Representative image showing starter neurons (yellow) that were restricted within the VLM. Scale bar: 100  $\mu$ m.

**D-E)** Representative images showing that neither CeA (D) nor BNST(E) provide excitatory inputs to the VLM. Scale bar: 200  $\mu$ m.

**Figure S7**

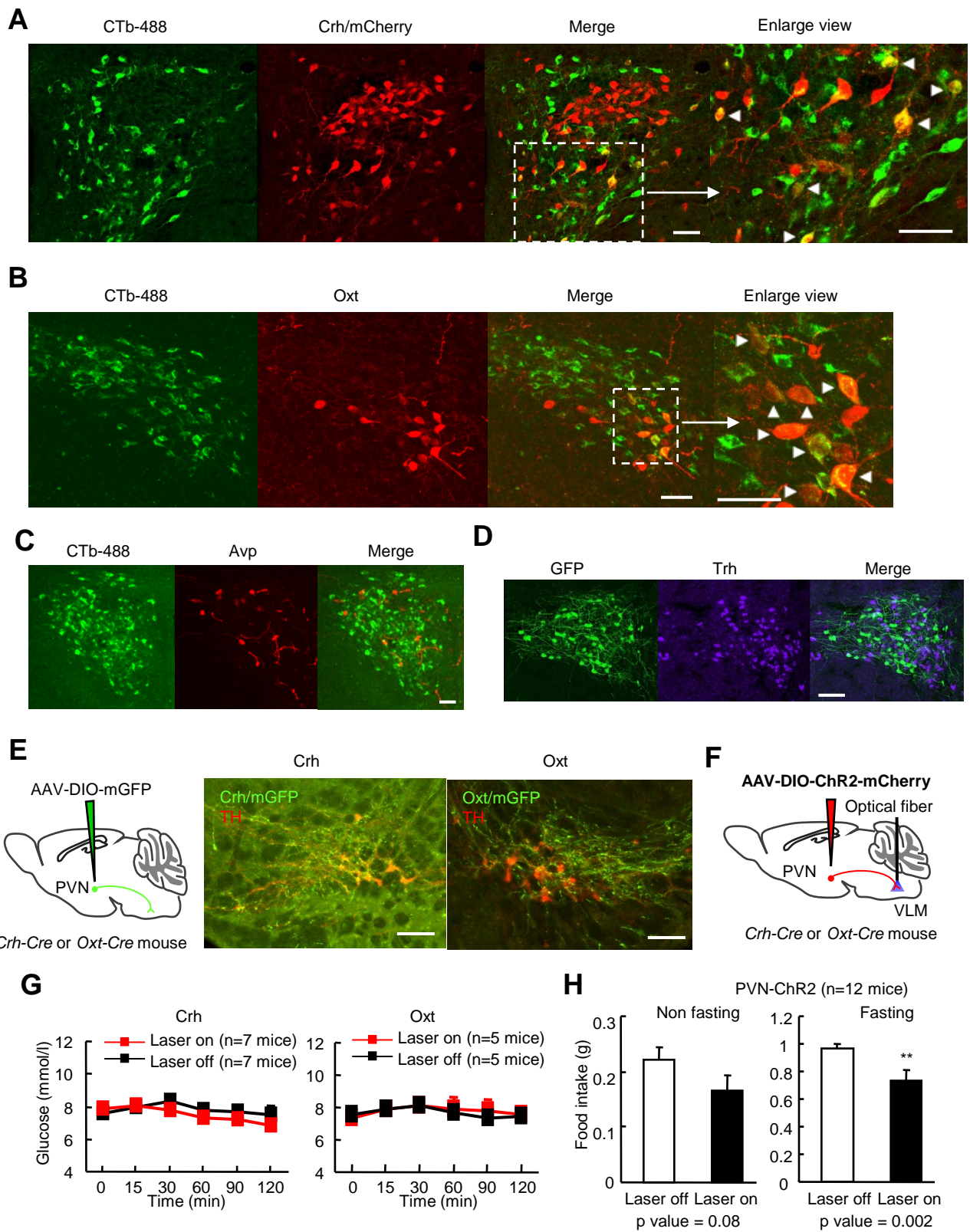


**Figure S7, related to Figure 7. Both Oxt and Crh neurons in the PVN project to the VLM.**

- A)** Representative images showing many CTb-488 (green) and Crh/mCherry (red) double-labeled neurons (indicated by triangles) following injection of CTb-488 into the VLM and injection of AAV-DIO-mCherry into the PVN of *Crh-ires-Cre* mice ( $n = 2$ ). Scale bar: 50  $\mu\text{m}$ .
- B)** Representative images showing that many Oxt-immunoreactive neurons (red, indicated by triangles) in the PVN were back-labeled by CTb-488 neurons (green) following the injection of CTb-488 into the VLM ( $n = 2$  mice). Scale bar: 50  $\mu\text{m}$ .
- C)** Representative images showing that none of Avp-immunoreactive neurons (red) in the PVN were back-labeled by CTb-488 (green) following injection of CTb-488 into the VLM ( $n = 2$  mice). Scale bar: 50  $\mu\text{m}$ .
- D)** Representative images showing that nearly none of Trh mRNA-expressing neurons (purple) in the PVN were GFP positive (green) following injection of rAAV2-hSyn-retro-eGFP into the VLM ( $n = 3$  mice). Scale bar: 100  $\mu\text{m}$ .
- E)** After injection of AAV-DIO-mGFP into the PVN of either *Crh-Cre* ( $n = 5$  mice) or *Oxt-Cre* mice ( $n = 5$  mice) (left panel), both Crh (middle panel) and Oxt (right panel) axonal projections (green) were observed in the VLM. Scale bar: 200  $\mu\text{m}$ .
- F-G)** After injection of AAV-DIO-ChR2-mCherry into the PVN of either *Crh-Cre* or *Oxt-Cre* mice (F), neither light illumination of Crh terminals ( $n = 7$  mice) nor illumination of Oxt terminals ( $n = 5$  mice) in the VLM can induce hyperglycemia (G). Two-way ANOVA analyses followed by Bonferroni's post hoc test for *Oxt-Cre* mice: Laser On/Off  $F(1,8) = 0.127$ ,  $p = 0.73$ ; time  $F(5,40) = 1.29$ ,  $p = 0.284$ ; interaction  $F(5,40) = 0.348$ ,  $p = 0.88$ . Two-way ANOVA analyses followed by Bonferroni's post hoc test for *Crh-Cre* mice: Laser On/Off  $F(1,12) = 1.908$ ,  $p = 0.192$ ; time  $F(5,60) = 2.997$ ,  $p = 0.017$ ; interaction  $F(5,60) = 0.884$ ,  $p = 0.497$ .
- H)** Optogenetic activations of PVN-derived glutamatergic terminals in the VLM of Vglut2-PVN<sup>ChR2</sup> mice ( $n = 12$  mice) has a minor but significant anorexic effect, in particular after overnight (12 hr) fasting. \*  $p < 0.05$ ; Student's t-test between groups.

# Supplemental Table

**Table S1, related to Figure 5. Brain areas innervated by VLM CA neurons.**

Brain areas	Fiber intensity	Brain areas	Fiber intensity
IML	****	VTA	**
Rob	**	ZI	***
NTS	****	LH	***
AP	**	PH	*
IRt	**	ARC	**
PMn	*	DMH	****
RPa	***	PVT	****
RMg	*	PVN	*****
LC	****	CeA	*
LPB	***	AH	**
SubC	***	MPO	***
DRN	**	VMPO	****
v1PAG	***	BNST	***
PSTh	**	LSV	**

Mean fiber intensity (0~255). \*: 1-30; \*\*: 30-60; \*\*\*: 60-90; \*\*\*\*: 90-120; \*\*\*\*\*: >120; -: null

## Abbreviation list of brain areas:

anterior hypothalamus (AH), area postrema (AP), arcuate nucleus (ARC), bed nucleus of the stria terminalis (BNST), central amygdaloid nucleus (CeA), dorsomedial hypothalamic nucleus (DMH), dorsal paragigantocellular nucleus (DPGi), deep mesencephalic nucleus (DpMe), dorsal raphe nucleus (DRN), alpha part of gigantocellular reticular nucleus (GiA), gigantocellular reticular nucleus (Gi), intermediolateral nucleus (IML), intermediate reticular nucleus (IRt), Kölliker-Fuse nucleus (KF), dentate cerebellar nucleus (Lat), lateral hypothalamus (LH), locus coeruleus (LC), lateral parabrachial nucleus (LPB), ventral part of lateral septal nucleus (LSV), medial amygdaloid nucleus (MeA), medullary reticular nucleus, dorsal part (MdD), medullary reticular nucleus, ventral part (MdV), medial preoptic area / nucleus (MPA / MPO), fastigial cerebellar nucleus (Med), nucleus tractus solitaires (NTS), periaqueductal gray (PAG), ventrolateral periaqueductal gray (v1PAG), parvicellular reticular nucleus (PCRt), posterior hypothalamic area (PH), paramedian reticular nucleus (PMn), caudal parts of the pontine reticular nucleus (PnC), oral parts of the pontine reticular nucleus (PnO), ventral parts of pontine reticular nucleus (PnV), parasubthalamic nucleus (PSTh), paraventricular hypothalamic nucleus (PVN), paraventricular thalamic nucleus (PVT), raphe obscurus nucleus (Rob), raphe magnus nucleus (RMg), raphe pallidus nucleus (RPa), red nucleus (Rn), subthalamic nucleus (STh), zona incerta (ZI), superior Colliculus (SC), primary somatosensory cortex (S1), subcoeruleus nucleus (SubC), ventromedial hypothalamic nucleus (VMH), ventromedial preoptic nucleus (VMPO), ventral tegmental area (VTA)